Sensors & Diagnostics

TUTORIAL REVIEW

View Article Online
View Journal | View Issue

Cite this: *Sens. Diagn.*, 2024, **3**, 599

Recent developments in ionophore-based potentiometric electrochemical sensors for oceanic carbonate detection

Stefanny N. Toala, [a] Zhentao Sun, [bc] Yanfeng Yue, *[a] Stephen F. Gonski[b] and Wei-Jun Cai*[b]

Received 6th September 2023,
Accepted 15th February 2024

DOI: 10.1039/d3sd00232b

rsc.li/sensors

The increasing level of atmospheric carbon dioxide (CO_2) driven by human activities contributes to the global concern of climate change. A consequence of these circumstances is ocean acidification, which reduces seawater pH. The increasing absorption of atmospheric CO_2 into the ocean decreases the concentration of carbonate ions and causes the sea to become more acidic, severely harming marine species. This harm to marine life has created the need for *in situ* carbonate sensing and monitoring to understand how marine ecosystems respond to pH reduction. Over the past few decades, many sensors with different compositions and structures have been developed to detect carbonate in seawater and other aquatic environments to simulate oceanic conditions. This review summarizes the recent developments in carbonate ionophores, a key component in carbonate electrochemical sensors, and compares the reported performance of these sensors through various parameters (*e.g.*, sensitivity, response time, lifetime, testing media, and measuring range). Current challenges within the development of carbonate ionophores and sensors and possibilities for future research are also discussed.

1. Introduction

The atmospheric level of carbon dioxide (CO_2) has been rising profusely since the Industrial Revolution with continual deforestation, cement production, and burning of fossil fuels.[1–3] As of February 2023, the global monthly average of atmospheric CO_2 peaked above 419 ppm, a 50% increase from preindustrial levels in 1750.[4,5] Approximately 25% of atmospheric anthropogenic CO_2 dissolves into the ocean each year.[6,7] While this oceanic absorption of CO_2 has mitigated climate change, the increase of aqueous CO_2 within seawater creates another environmental concern called ocean acidification.[8] When CO_2 dissolves in seawater, it causes an equilibrium shift between the inorganic carbon species by shifting the net reaction, $H_2O + CO_2 + CO_3^{2-} \rightarrow 2HCO_3^-$, to form more bicarbonate (HCO_3^-).[9–11] As a result, carbonate ion concentration [CO_3^{2-}] decreases while the proton ion concentration [H^+] and bicarbonate ion concentration [HCO_3^-] increase, which lowers the pH of the water.[12] A decreasing seawater pH can alter the rates of redox reactions and the availability of metals and nutrients essential to biological processes.[13–17] For example, a lowering pH leads to a reduction of the carbonate mineral saturation state (Ω), which is mainly controlled by the [CO_3^{2-}].[9,18,19] Thus, the decline of CO_3^{2-} directly decreases the potential for calcite and aragonite mineral formation ($CO_3^{2-} + Ca^{2+} \rightleftharpoons CaCO_3$).[12] Decreased production of these minerals negatively impacts the ability of marine calcifying organisms (*e.g.*, coral, crustaceans, and shellfish) to form their shells or skeletons.[20–24] As a result, reduced calcification and growth rates for calcifying organisms have been observed, which alters their function in marine ecosystems.[25,26]

This harm to marine life has motivated new research efforts in ocean chemistry, including developing reliable and low-cost methods to monitor CO_3^{2-} levels for ocean acidification research. Substantial advancements have been accomplished in the *in situ* sensing of CO_2 and pH; however, reliable *in situ* CO_3^{2-} sensing is still lacking.[27,28] It is crucial to develop highly selective, sensitive, and stable sensing devices capable of monitoring [CO_3^{2-}] to study ocean acidification and understand how marine organisms respond. Carbonate sensors may also lead to advancements in biological applications (*e.g.*, disease screening and personalized medicine) since carbonate is also present in clinical samples.[29] A few demonstrations of *in situ* carbonate sensing have been reported and reviewed; however, this review addresses the potential that carbonate electrochemical sensors based on novel carbonate ionophores have to be

[a] *Department of Chemistry, Delaware State University, Dover, DE 19901, USA. E-mail: yyue@desu.edu*
[b] *School of Marine Science and Policy, University of Delaware, Newark, DE 19716, USA. E-mail: wcai@udel.edu*
[c] *Ocean College, Zhejiang University, Zhoushan 316021, China*

highly selective, sensitive, and stable in the marine environment.[30–32] This review comprehensively summarizes and compares recent advancements within carbonate electrochemical sensors based on novel carbonate ionophores, including a discussion on ionophore characterization, membrane fabrication, and sensor evaluation. The current challenges within the development of carbonate ionophores and sensors and possibilities for future research are also discussed. Research on ocean acidification will continue to be relevant for protecting the environment, ensuring a promising and healthier aquaculture industry, and supporting the development and large-scale implementation of ocean-based carbon dioxide removal (CDR) technologies.[33]

2. Seawater carbonate chemistry and method of indirect $[CO_3^{2-}]$ determination

The carbonate system in seawater serves as the ocean's primary pH buffer through carbon dioxide gas-water equilibrium reactions.[34,35] When atmospheric CO_2 dissolves into seawater, aqueous CO_2 is formed. Aqueous CO_2 reacts with water molecules in the ocean to form carbonic acid (H_2CO_3), which gradually dissociates into HCO_3^- and H^+ ($H_2O + CO_2 \rightleftharpoons H_2CO_3 \rightleftharpoons HCO_3^- + H^+$).[34] The newly formed HCO_3^- can also dissociate, forming CO_3^{2-} and more H^+ ($H_2O + CO_2 \rightleftharpoons HCO_3^- + H^+ \rightleftharpoons CO_3^- + 2H^+$).[36] The spike in H^+ concentration lowers ocean pH; however, the ocean attempts to mitigate the rise in acidity by limiting the dissociation of HCO_3^- ($H_2O + CO_2 + CO_3^{2-} \rightarrow 2HCO_3^-$) and shifting the equilibrium between HCO_3^- and CO_3^{2-} ($HCO_3^- \rightleftharpoons CO_3^{2-} + H^+$). Through the equilibrium shift, some of the excess H^+ are consumed to form more HCO_3^-, causing the drop in pH to be smaller than it would be in an unbuffered system.[9] While this protects the ocean from greater declines in pH, this process consumes CO_3^{2-} and decreases its availability to form calcite and aragonite minerals through the carbonate mineral saturation state ($CO_3^{2-} + Ca^{2+} \rightleftharpoons CaCO_3$). Reduced production of these minerals harms marine life, especially marine calcifying organisms.[12] Overall, the increase of aqueous CO_2 in seawater due to increasing atmospheric CO_2 is causing the ocean to continually buffer increasingly higher H^+ concentrations, which steadily lowers ocean pH. Research models predict ocean pH will drop to 7.8 or 7.7 by the end of this century if seawater continues to absorb CO_2 at the current rate.[37] To understand how marine ecosystems are responding to reduced pH, it has become increasingly important to monitor the $[CO_3^{2-}]$ in the ocean.

At equilibrium, the concentrations of aqueous CO_2, HCO_3^-, and CO_3^{2-} are written in terms of two equilibrium constants:

$$K_1 = \frac{[H^+][HCO_3^-]}{[CO_2]} \quad (1)$$

$$K_2 = \frac{[H^+][CO_3^{2-}]}{[HCO_3^-]} \quad (2)$$

Which are also referred to as the first and second dissociation constants of carbonic acid.[36] Since carbonic acid is a weak and unstable acid only occurring in aqueous solutions, the chemical and biochemical reactivity of the compound is not completely known.[34] As a result, the precise values of K_1 and K_2 are subject to great debate.[38] Despite this uncertainty, past research has relied on mathematical relationships using published values of these constants and other analytical parameters to study seawater carbonate chemistry since measuring individual concentrations of acid–base species in seawater is difficult.[39]

Consequently, the study of marine carbonate species has been accomplished through seawater sample collection during hydrography cruises and the mathematical relationships between four analytical parameters, including pH, total dissolved inorganic carbon (DIC), total alkalinity (TA), and CO_2 fugacity or partial pressure (f_{CO_2} or pCO_2).[26,40–44] Using the thermodynamic equilibrium relations of these parameters and the measured values of any two parameters, $[CO_3^{2-}]$ can be calculated along with the remaining unknown parameters.[45] However, *in situ* temperature, salinity, and the concentrations of minor acids and bases are also needed for the calculation.[46] These variables are not always measured or known, which severely lessens the reliability of the calculation since the K_1 and K_2 constants depend on *in situ* salinity and temperature.[39,42] To obtain a highly accurate $[CO_3^{2-}]$ and examine internal consistency, all four parameters are required for the calculation; however, time, staff, and instrumentation typically allow for only two of them to be measured.[47] Comparison of $[CO_3^{2-}]$ determined from various pairs of parameters (*e.g.*, pH and TA *versus* DIC and pCO_2) are subject to inaccuracies, increasing the challenges of using this indirect method of $[CO_3^{2-}]$ determination.[48] Overall, three issues seriously impede our ability to obtain an accurate $[CO_3^{2-}]$ *via* the calculations from these parameters: 1) propagation of errors in isolated analytical methods, 2) the lack of knowledge of the organic acid contributions to alkalinity as part of the inorganic carbon model, and 3) a notable uncertainty in the first and second dissociation constants (K_1 and K_2) of carbonic acid in seawater and brackish waters.[42,49–52] As a result, ocean acidification research has moved toward the development of *in situ* carbonate sensors to capture more accurate $[CO_3^{2-}]$.

3. *In situ* measurements for $[CO_3^{2-}]$ determination

3.1 The need for *in situ* measurements

The indirect method to determine $[CO_3^{2-}]$ briefly discussed in section 2 requires water sample collections at defined locations and depths before samples are transported, stored, and then later analyzed in a laboratory after a costly

pretesting procedure performed by well-trained personnel.[53,54] Based on the need for pretesting procedures and experienced personnel, this aggregate procedure is costly and disadvantageous. Furthermore, analytical methods that depend on collecting and analyzing discrete samples seldom produce representative datasets with enough data points for high spatial and temporal resolution to fully capture substantial simultaneous changes in temperature, salinity, and biogeochemistry that characterize marine ecosystems.[55]

Conversely, *in situ* analysis is an approach that can create high spatial and temporal resolution data sets and satisfy the need for real-time measurements. *In situ* measurements are those taken instantaneously at the given location, alleviating most of the logistical and economic challenges of sampling, pretesting procedures, and analysis.[53] Additionally, this process reduces limitations imposed by humans who may be unable to reach specific locations (*i.e.*, various depths within the ocean or in ice-covered water).[56] For these reasons, building *in situ* sensors for carbonate detection is vital to advancing ocean acidification and marine carbonate chemistry research.

3.2 Evaluating sensor types and their potential for oceanic *in situ* carbonate detection

Over the years, sensors based on the Severinghaus electrode, and others based on optical, voltametric, and potentiometric principles have been explored for ocean studies. The Severinghaus electrode consists of a pH electrode in contact with a thin layer of bicarbonate solution that is separated from the sample by a gas permeable membrane to measure dissolved CO_2. With this setup, dissolved CO_2 in the sample can diffuse through the membrane into the inner $NaHCO_3$ solution, where pH changes occur until an equilibrium is established. The resulting pH of the bicarbonate solution in contact with the electrode correlates to dissolved CO_2 levels in the sample.[57] While these electrodes are relatively inexpensive and easy to handle, this sensor design has drawbacks that deem it unsuitable for oceanic *in situ* detection. Since this design requires equilibrium establishment before measurement, the response time cannot be suitably shortened to capture minute changes in analyte concentration.[57] In addition, these sensors require a careful calibration process, and still exhibit sensitivity that is not ideal for seawater analysis.[57,58] Considering ocean acidification research, Severinghaus based sensors cannot currently detect carbonate and are unlikely to collect the data necessary for high resolution data sets.

Similarly, current optical sensors (*e.g.*, optodes) are incompatible with the goals of ocean acidification research. Recently, many optodes have been tested in seawater and other natural waters.[59–64] The working principle of this sensor type relies on the mass transfer between the sensing material and sample. Mass transfer can occur through ion-exchange between the target analyte and a reference ion (*e.g.*, a proton) or the co-extraction of the target analyte and a counter ion in the sensing phase.[59] In either case, the protonation of the indicator dye correlates to analyte concentration.[60] Even though these sensors contain favorable characteristics (*e.g.*, small size, versatility, ease of use, low drift, fast response time, and long lifetime), these sensors have only detected pH and dissolved O_2 and CO_2.[61–64] Furthermore, the issue of Cl^- interference has been reported.[59]

Electrochemical sensors, including voltametric and potentiometric sensors, have also been tested for ocean-based research. Potentiometric electrochemical sensors are the focus of this review, and their working principle is deeply covered in section 4. Unlike potentiometric sensors, voltametric sensors require a counter electrode along with a working and reference electrode in their structure. From voltametric sensors, qualitative and quantitative information of an active redox analyte can be obtained by measuring the current as the potential in the 3-electrode cell is varied.[65] The type of voltammetry used (*e.g.*, cyclic voltammetry, differential pulse voltammetry, square wave voltammetry, and chronoamperometry) depends on how the potential is varied. Current voltametric sensors for ocean-based research can measure pH and various trace metals (*e.g.*, Zn^{2+}, Cd^{2+}, and Pb^{2+}) and ions (*e.g.*, NO_3^-, NO_2^-, HPO_4^{2-}, PO_4^{3-}, and $H_2PO_4^-$).[37,66–76] While these sensors have great analyte versatility, no voltametric sensors currently detect carbonate and sensor lifetime is limited.[37,65] The lifetime of these sensors depends on the number of measurements recorded by the electrode, and frequent measurements age the electrode until peak potential cannot be reached.[37] Thus, voltametric sensors may require maintenance too frequently for long-term oceanic *in situ* carbonate detection.

Currently, a few true demonstrations of *in situ* electrochemical sensors have been reported, even in seawater applications.[65] To the best of our knowledge, the most recent sensor capable of oceanic *in situ* measurement is a submersible potentiometric probe composed of a flow cell based on miniaturized solid-state sensors that can measure pH and the concentrations of carbonate and calcium ions in seawater.[31] Based on previous success, potentiometric electrochemical sensors currently demonstrate the most promise for ocean acidification research. Not only can these sensors detect carbonate, but also pH, dissolved CO_2, and bicarbonate, which can all be used to study marine carbonate chemistry and ocean acidification.[30,77] A recently developed novel potentiometric sensor for dissolved CO_2 detection resolves issues frequently encountered using classical Severinghaus CO_2 probes.[30] The sensor created by Athavale and co-workers is based on EMF measurement between two solid-contact ISEs, a hydrogen selective sensor, and a carbonate selective senor and collects high resolution *in situ* data with insensitivity to changes in pressure and a response time of less than 10 seconds in freshwater lakes. Another recent advancement in the potentiometric sensing of dissolved CO_2 and bicarbonate came from Li and co-workers.[77] Their sensor is capable of sensing bicarbonate and

dissolved CO_2 in mineral water and beverage samples using neutral and charged calix[4]pyrroles with *meso*-substituted groups as ionophores. Based on these examples, potentiometric electrochemical sensors can be modified for various applications and have immense potential for the *in situ* detection of carbonate and other analytes crucial for monitoring ocean acidification. However, various challenges still complicate the wide-spread implementation of these devices for ocean acidification research (discussed later in section 4.3). As of June 2021, the European Marine Board stated that substantial progress is needed before *in situ* ocean observations can be incorporated into the global ocean observation system.[78] Despite several unknowns in manufacturing and evaluating these robust devices, current research has compiled expected attributes for *in situ* electrochemical sensors that monitor natural waters such as seawater.[79,80] The ideal sensor should simultaneously identify and quantify the concentration of a selected species (*e.g.*, carbonate) while being small, simple, and relatively inexpensive. Additionally, the sensor should remain stable and not alter the sample composition during the test period.[81] These sensors may require new technology and analytical or biophysical concepts to meet these standards, so the challenge of creating robust *in situ* electrochemical sensors will remain for several years.[81]

4. Electrochemical sensors for carbonate detection

4.1 The basis of electrochemical sensors

Electrochemical sensors can convert reactions between an electrode and a specific analyte into readable signals.[82] Typically, these signals originate following changes in chemical and electrical interactions.[82] However, a change in physical properties may also result in a signal.[83] In its most basic form, the electrochemical sensor consists of a receptor unit, a sample containing an analyte, and a transducer (*e.g.*, an electrode), which work together to produce a signal corresponding to the measurement of interest.[83,84]

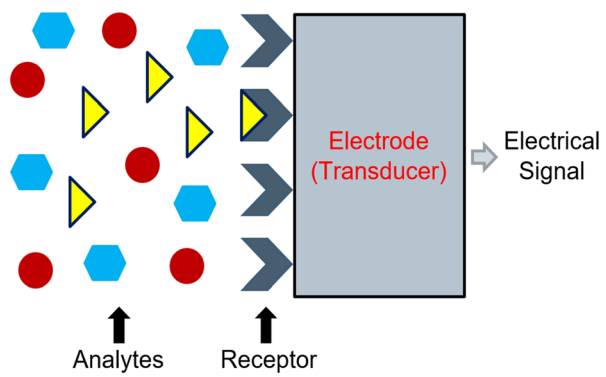

Fig. 1 Representation of the working principle of an electrochemical sensor which operates based on a chemical reaction between a receptor unit and a specified analyte.

Frequently, the signal corresponds to the activity of a target ion, and its strength will adjust based on the measured activity.[84] Commonly, the receptor unit manifests as a membrane that should only interact with the target ion. When the membrane interacts with the target ion, it should alert the electrode to produce an assessable signal (Fig. 1).

4.2 Electrochemical sensors based on potentiometry

Potentiometric electrochemical sensors create a potentiometric cell where the potential difference at equilibrium (*i.e.*, at zero current) between two electrodes relates to an analyte's activity.[85] Because of this, these sensors may also be called potentiometric ion sensors.[86] In the composition of a potentiometric electrochemical sensor, an external reference electrode (ERE) and an ion-selective electrode (ISE) are connected to a voltmeter (Fig. 2).

4.2.1 The definition of ion-selective electrodes. Ion-selective electrodes (Fig. 2c) are the core piece of the potentiometric electrochemical sensor as the working electrode. They consist of three components, including an internal reference electrode (Fig. 2d), an internal reference solution (Fig. 2e), and an ion-selective membrane (Fig. 2f).[82,86,87] The ion-selective membrane acts as the receptor unit previously described, so its composition must be permeable to only the target ion.[86,87] The fabrication of ion-selective membranes is further discussed in section 6. For the ion-selective electrode to function accurately, the internal reference solution must contain the target analyte, and the electron conductivity of the membrane should be imperceptible within the condition of measurement.[85,87]

4.2.2 The theory of potentiometric response. As shown in Fig. 2, the ERE and ISE must be plunged into the sample solution. The ERE should maintain a constant potential with

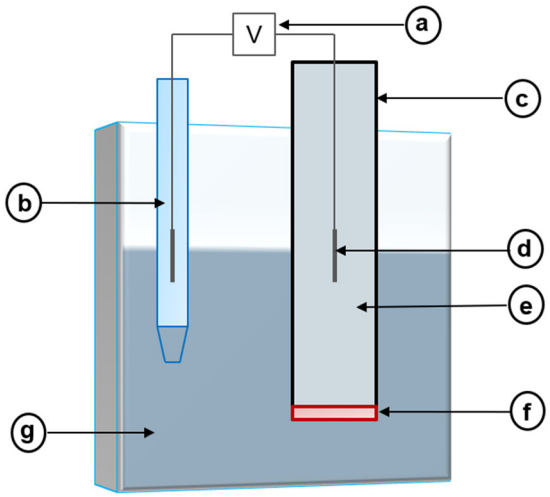

Fig. 2 Representation of a potentiometric cell which consists of the following components: voltmeter (a), reference electrode (b), ion-selective electrode (c) which contains an internal reference electrode (d), an internal solution (e) and an ion-selective membrane (f), and sample solution (g).

the sample.[85] However, ions can migrate between the ERE and the sample, creating a liquid–liquid junction that produces junction potential.[85,88] If the junction potential is too high and variable, measurement error can occur.[89] Considering the presence of junction potential, the cell potential of a potentiometric cell can be represented and measured by:

$$E_{\text{cell}} = E_{\text{ISE}} - E_{\text{ERE}} + E_{\text{J}} \quad (3)$$

where E_{cell} is the cell potential, E_{ISE} is the potential of the ISE, E_{ERE} is the potential of the ERE, and E_{J} is the potential of the liquid junction.[85] Salt bridges can minimize liquid junction potential; however, they may not completely prevent the loss of electrolytes into the sample and the contamination of the salt bridge by the sample.[90] Porous plugs with low electrical resistance are an alternative for salt bridges by providing additional stability while maintaining electrical contact between the electrode and the sample.[90,91]

Assuming the liquid junction potential is correctly limited and stable, the potential of the ISE can be measured against the ERE. The potential of the ISE is controlled by the potential of the internal reference electrode (E_{IRE}) and the ion-selective membrane (E_{membrane}).[85] Thus, eqn (3) can be rewritten as:

$$E_{\text{cell}} = E_{\text{IRE}} + E_{\text{membrane}} - E_{\text{ERE}} + E_{\text{J}} \quad (4)$$

When the ISE is in contact with the sample solution, the E_{IRE} is constant since the inner ion-selective membrane surface is in contact with a constant target ion activity through the internal reference solution. Conversely, the potential difference between the sample and the outer membrane surface (E_{membrane}) depends on the activity of the target analyte in the sample. Assuming that E_{IRE} and E_{ERE} are constant and E_{J} is minimized, E_{cell} depends on E_{membrane}. The difference in potential across the membrane can be calculated through the Nernst equation:

$$E_{\text{membrane}} = 2.303\frac{RT}{zF}\log\frac{a_{\text{i.sample}}}{a_{\text{i.reference}}} \quad (5)$$

where E_{membrane} is the potential of the membrane, R is the ideal gas constant, T is the temperature, z is the charge carried by the target ion i, F is Faraday's constant, $a_{\text{i.sample}}$ is the activity of the target ion i in the sample, and $a_{\text{i.reference}}$ is the activity of the target ion i in the internal reference solution.[85,92–94] Since E_{membrane} depends on $a_{\text{i.sample}}$, E_{cell} can also be represented by this equation:

$$E_{\text{cell}} = E' + 2.303\frac{RT}{zF}\log a_{\text{i.sample}} \quad (6)$$

where E' is the measuring sequence's standard potential, which takes all potentials into account.[85] The activity of the target ion (a_{i}) is related to its concentration (C_{i}) through the following equation:

$$a_{\text{i}} = \gamma_{\text{i}} C_{\text{i}} \quad (7)$$

where γ_{i} is the activity coefficient based on the total ionic strength I, which represents the sum of the charge of all ions present in the medium, through the Debye–Hückel equation:

$$\log\gamma_I = -0.5 z_{\text{i}}^2\sqrt{I} \quad (8)$$

This version of the Debye–Hückel equation is only applicable when I is less than 0.001 M.[95] For higher total ionic strengths, where $I \leq 0.1$ M, the extended Debye–Hückel equation must be used:

$$\log\gamma_I = \frac{-Az_{\text{i}}^2\sqrt{I}}{1 + B\mathring{a}\sqrt{I}} \quad (9)$$

where A and B are constants dependent on temperature and pressure and $\mathring{a}$ is the radius of the ion in angstroms.[95] Based on eqn 7 and 8, eqn 6 can be rewritten and E_{cell} can depend on the target analyte's concentration through the following equation:

$$E_{\text{cell}} = E'' + 2.303\frac{RT}{zF}\log C_{\text{i}} \quad (10)$$

Assuming that the γ_{i} and I have been stabilized through the addition of an ionic strength adjusting buffer.[85,96] Overall, the Nernst equation represents the quantitative relationship between a potentiometric cell's potential and the activity of a target ion in theoretical conditions, so the measurements based on this equation describe the ideal response.[97] Hence, the Nernst theoretical slope of −29.6 mV per decade or 59.2 mV/z is frequently compared to the experimental response slope to explain whether Nernstian behavior occurred.[98,99]

4.3 The current challenges surrounding *in situ* carbonate electrochemical sensors and measurements

Potentiometric response from potentiometric electrochemical sensors is complex. This type of response is a time-dependent process mainly controlled by the ion-selective membrane and the sample. The interface at which the membrane and sample meet consists of various properties that depend on the composition of the two. However, other factors also affect potentiometric response and create challenges in developing *in situ* carbonate electrochemical sensors and documenting [CO_3^{2-}] long-term.[86]

4.3.1 The problem of activity *versus* concentration. Based on the Nernst equation (eqn (5)), ISEs can directly measure analyte activity, not concentration.[96] In some applications (*e.g.*, clinical and physiological applications), ion activity is beneficial; however, in other applications (*e.g.*, ocean acidification research and other environmental applications), ion concentrations are preferable for analysis and validation.[100] Thus, a reliable method for measuring ion concentration from potentiometric response is needed. Since ion activity and concentration depend on ionic strength (eqn (7)–(9)), a known ionic strength makes a reliable conversion between ion activity and concentration possible. However, the ionic strength of a sample is not always known or

constant, especially in real-time detection and remote sensing applications, including ocean acidification research. Additional steps are required before converting ion activity to concentration, including a correction for liquid junction potential and an ionic strength adjustment by adding a buffer to the sample.[100] Following these steps, ion activity can be converted to concentration using the connections between eqn (7) and (8) or (9) and (10). Even though this method can successfully result in concentration measurements from potentiometric response, developing a potentiometric cell capable of directly measuring ion concentration is ideal to avoid complications surrounding liquid junction potential and ionic strength. Two examples of direct potentiometric sensing of ion concentrations exist; however, they are not currently designed for divalent anions like carbonate.[96,100]

4.3.2 Structural components capable of limiting sensor capabilities. A liquid junction and its potential can cause measurement errors, but it can also cause the sensor to be mechanically fragile. A mechanically vulnerable sensor may rupture the ion-selective membrane and compromise the ISE. In this scenario, the internal reference solution would leak directly into the sample, skewing the measurements since this solution must contain the target analyte.[85] Because of this possibility, it is crucial to limit junction potential to ensure sensor functionality and measurement reliability.

The composition of the internal reference solution is another structural component that can affect sensor functionality due to its potential to cause transmembrane ion fluxes.[101,102] Theoretically, the composition of the internal reference solution should maintain the internal reference electrode's constant potential and generate no concentration gradient by allowing the same amount of target analyte and interfering ion to replace each other on both sides of the membrane.[103] However, concentration gradients can arise if interfering ions replace the target analyte within the membrane, allowing target analytes from the membrane to leach into the sample. Once the target analytes flux into the sample, a significant difference between the concentration of the target analyte near the membrane and in the entire sample emerges and skews measurement readings. This negatively impacts the sensor's lower detection limit and selectivity (discussed in depth in section 7).

The possibility of transmembrane ion fluxes also depends on the sample composition. Any changes in the sample can also cause concentration gradients that lead to ion fluxes.[104] Changes in samples frequently occur in environmental samples (*e.g.*, ocean water samples at various locations and depths), so the design and optimization of the internal reference solution is critical to limit ion fluxes. Some strategies for optimizing internal reference solutions include lowering the concentration of ionic sites and adjusting the composition to induce ion exchange like a typical sample would.[104,105] Adjustments to the ion-selective membrane can also reduce the prevalence of ion fluxes. These adjustments include increasing the thickness or polymer content of the membrane and designing it to be as resilient to concentration gradients as possible.[103–105] Other potential avenues for avoiding ion fluxes include using a flow-through cell or rotating electrodes, using internal solution-free sensors (*e.g.*, solid state ISEs), and covalently bonding the ionophore to the polymer backbone of the membrane.[102,104,106–108] The ionophore and its role in ion-selective electrodes are discussed in depth in section 5. Additional drawbacks with using an internal reference solution include its sensitivity to changes in temperature and pressure, which may cause the solution to evaporate and lead to the delamination of the ion-selective membrane.[109]

4.3.3 Oceanic conditions capable of limiting sensor capabilities. The ocean is an unwelcoming environment for foreign entities, and its natural conditions complicate long-term sensor deployment. Sensor deployment is often shortened because of biofouling. Biofouling is the accumulation of natural substances (*e.g.*, algae, plants, and microorganisms) on the device, which may cause damage to the sensor and its membrane, preventing the capture of accurate long-term measurements.[32] Sensors in oceanic or oceanic-like environments also experience interference from other ions in natural waters (*e.g.*, SO_4^{2-}, Cl^-, ClO_4^-, SCN^-, NO_3^-, NO_2^-, Br^-, and HPO_4^{2-}). As a result, a sensor's ability to detect carbonate over other anions is fundamental for a successful *in situ* carbonate electrochemical sensor. Another aspect of oceanic conditions that must be considered is pH, especially as ocean acidification causes seawater to become more acidic. The potentiometric response and resultant response slope are likely sensitive to pH changes. Past studies report that using a buffer to increase pH can result in a more favorable response slope; however, there are examples where pH changes in samples did not substantially affect potential response.[110–113] The effect of pH on an electrochemical sensor is highly variable based on the sensor type and structure. Because of this, sensors should be tested at average ocean pH (8.1) and lower to ensure their practical application for ocean acidification research. Overall, the ocean is a vast environment of varying temperature, salinity, and pressure. Building a sensor capable of handling different temperatures, salinities, and pressures while maintaining stability and functionality is a fundamental challenge within ocean research.[109] There are currently few demonstrations of oceanic sensors capable of operating in deep-sea conditions.[98,114]

4.3.4 The lack of method validation. Despite the consensus on the value of *in situ* measurements and sensors, no method has been agreed upon to ensure the quality of these measurements (*e.g.*, uncertainty estimation). The infancy of these sensors, the varying conditions of the ocean, and the time required to develop instrumentation have complicated the validation of measurements. Currently, validation protocol for general oceanic sensors is used for *in situ* oceanic sensors.[79] The present best practices are extensively described.[115–118] However, a uniform quality assurance and control protocol should be set for *in situ*

sensors in various oceanic conditions to produce adequate, reliable data for understanding ocean carbonate chemistry.

5. Ionophores for carbonate detection

5.1 The definition of an ionophore and the framework of carbonate ionophores

An ionophore must be within the composition of the ion-selective membrane for the membrane to be selectively permeable to a target analyte. An ionophore is a substance capable of binding and transporting a particular ion through a membrane. Since the ionophore facilitates the identification and transport of the target ion, it must be highly selective and sensitive to the target. A carbonate ionophore capable of transporting only carbonate ions through the ion-selective membrane is needed to advance *in situ* carbonate electrochemical sensors for ocean acidification research.[119]

Research completed by Wise, Herman, and Rechnitz notably provides the framework of the carbonate ionophore. In 1973, Wise reported trifluoroacetylbutylbenzene (TFABB) as an ionophore for bicarbonate detection using bicarbonate ISEs.[120] Later, Herman and Rechnitz detailed that TFABB was most likely sensing carbonate instead of bicarbonate. With this ionophore, Nernstian behavior was present in the concentration range of 10^{-2} to 10^{-7} M of carbonate ions, and the sensor had a quick response time and an overall low noise level.[121] Since these initial findings, various types of carbonate ionophores have been investigated, including small organic molecules, molecular tweezers, and metal-based complexes.

5.1.1 Small organic molecules as carbonate ionophores. Within the category of small organic molecules, neutral carriers and charged carriers are prospects for carbonate ionophores. Neutral carriers are ionophores that contain no charge when it has not bonded with the analyte, whereas charged carriers are ions before the interaction occurs.[122] Neutral carriers have been frequently used for many applications within ISEs, including clinical, industrial, and environmental applications.[123]

For some time, trifluoroacetophenones (TFAs), which include TFABB, were the only group of molecules identified as carbonate ionophores.[124] Besides carbonate, TFAs can also sense propionate, lactate, benzoate, salicylate, phenylpyruvate, amino acids, sulfate, and phosphate.[125–132] The ability of TFAs to act as ionophores for various target ions attests to the usefulness of these compounds; however, it also explains the challenges researchers have reported with their sensors experiencing interference from other ions.

For TFAs, three possible mechanisms exist to explain how these molecules sense carbonate. Scott and co-workers suggest two mechanisms through studies of TFA-based polymeric membranes.[133] Tetrahedral nucleophilic adducts can form after carbonate binds the carbonyl carbon on TFA (Fig. 3a), or hydrogen bonding between a hydrated TFA and carbonate can create carbonate-ionophore complexes (Fig. 3b). The third mechanism also involves the formation of hydrogen bonding but considers the effective charge on the carbonyl carbon in TFA (Fig. 3c). Considering the effective charge on the carbonyl carbon, hydrogen bonding would form between the phenyl hydrogens of TFA and carbonate.[134] Through energy analysis and stoichiometric studies of all three mechanisms, Makarychev-Mikhailov and co-workers suggest that the hydrogen bond complex formation is the most realistic mechanism; however, Meyerhoff and co-workers report the occurrence of carbonate sensing through the nucleophilic adduction mechanism.[124,135]

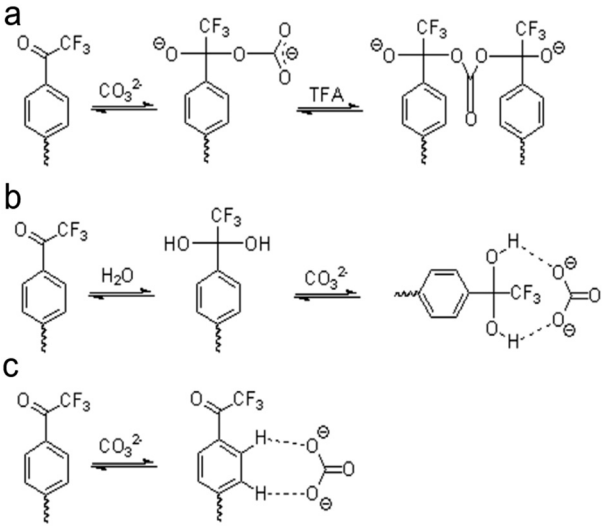

Fig. 3 Representation of proposed mechanisms for carbonate sensing through TFA-based polymeric membranes: (a) the formation of tetrahedral nucleophilic adducts, (b) the formation of hydrogen bonds by nucleophilic addition, and (c) the formation of hydrogen bonds based on the effective charges of the carbonyl carbon.

Even though TFA-based membranes can sense carbonate, the sensors exhibited a low selectivity and lipophilicity, a short lifetime (*e.g.*, a couple of days), and a high detection limit.[120,136] These disadvantages motivated researchers to modify the structure of TFA to determine whether any alteration could potentially alleviate the drawbacks. Research has explored placing substituents (*e.g.*, hexyl, nitro, bromo, and carboxyl substituents) in the *para*-position, which corresponds to position 4 on the phenyl ring of TFA (Fig. 4a).[137–139] Modifying the *para*-position of the ring affects the acidity of the group responsible for detecting carbonate and modifies the compound's ability to bind carbonate. Based on comparisons of lipophilicity, the carboxyl substituent may be the most promising due to a high Hammett constant value, which reflects its ability to potentially increase lipophilicity.[136] Lipophilicity can impact selectivity depending on the presence of a lipophilic cation or anion. For example, cationic selectivity would be hindered if a lipophilic cation is present within a membrane.[138]

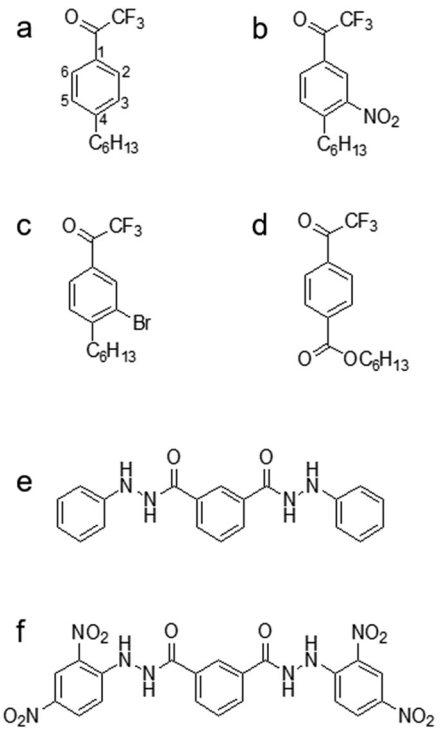

Fig. 4 Small organic ionophores. TFA-derivatives: (a) 4-hexyltrifluoroacetophenone (Hex-TFA); (b) 3-nitro-4-hexyltrifluoroacetophenone (NO_2-TFA); (c) 3-bromo-4-hexyltrifluoroacetophenone (Br-TFA); (d) hexyl-4-trifluoroacetyl benzoate (HE). Diamide derivatives: (e) *N*,*N*^{I}-bis(phenyl) isophthalohydrazide; (f) *N*,*N*^{I}-bis(2,4-dinitrophenyl)isophthalohydrazide. On ionophore *a*, the carbon atoms are labeled to explain which position(s) of the substituent corresponds to *para* and *meta* substitution.

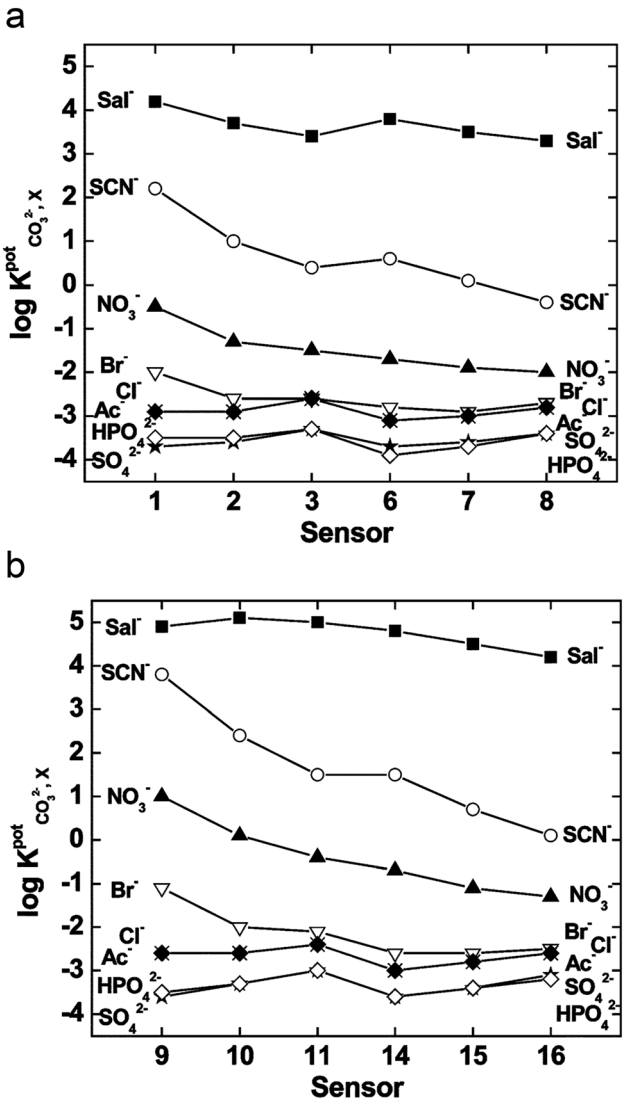

Fig. 5 Selectivity of the sensors for various ions tested with membranes plasticized with bis(2-ethylhexyl)sebacate (a) and 2-nitrophenyloctyl ether (b), where the *x*-axis represents a sensor labeled by number designated by the authors in the original work. Used with permission from Royal Society of Chemistry 2004; permission conveyed through Copyright Clearance Center, Inc.[124]

Substituents in the *meta*-position, which correspond to positions 3 or 5 on the phenyl ring (Fig. 4a), have also been evaluated. Makarychev-Mikhailov and co-workers built carbonate sensors using 4-hexyltrifluoroacetophenone (Hex-TFA) and its 3-nitro- (NO_2-TFA) and 3-bromo- (Br-TFA) derivatives as ionophores. Hexyl trifluoroacetylbenzoate (HE) was used as a control to determine the effect of *meta*-position substituents on carbonate selectivity.[136] The structures of Hex-TFA, NO_2-TFA, Br-TFA, and HE are in Fig. 4. Results displayed that the $-NO_2$ and –Br substituents increased the Lewis acidity of the fluoroketone group and the carbonate selectivity. The *meta* substitution of $-NO_2$ resulted in increased carbonate selectivity, especially with NPOE-plasticized membranes; however, a higher detection limit and pH sensitivity greatly limit the practical use of this ionophore.[136] The pH sensitivity eliminates this molecule as an effective carbonate ionophore for ocean acidification research. However, the *meta* substitution of –Br was similar in response to the control, which makes it appealing for future research.[136] From these results, Makarychev-Mikhailov and co-workers moved to test TFA as a carbonate ionophore while containing bromo- and nitro-substituents simultaneously.[124]

Compared to the mono-substituted TFA, the double *meta*-substituted TFA had a higher carbonate selectivity than Br-TFA and higher lipophilicity than NO_2-TFA. The lipophilicity increased by 0.5, positively impacting the detection limit and electrode lifetime.[124] In addition, an increasing trend of carbonate selectivity against interferents (*e.g.*, salicylate (Sal$^-$), thiocyanate, and nitrate) occurred as ionophore concentration increased (Fig. 5).[124]

Along with TFAs, hydrazides and their various forms have been assessed. *N*,*N*^{I}-Bis(phenyl)isophthalohydrazide and *N*,*N*′-bis(2,4-dinitrophenyl)isophthalohydrazide (Fig. 4e and f), were mainly tested against the interferent Sal$^-$. The potential of the sensor was measured as a function of carbonate activity while set concentrations of Sal$^-$ ions were added into the sample (1.0×10^{-4}, 1.0×10^{-3}, and 5.0×10^{-3} M).[140] The potentials obtained from samples containing CO_3^{2-} and Sal$^-$

versus those containing only CO_3^{2-} remain identical until a distinct divergence point (Fig. 6), which indicates the presence of Sal^- interference and marks the measuring range of the sensor for carbonate sensing.[140]

Comparing both ionophores (Fig. 4e and f), ionophore f allows for a broader measuring range, a shorter response time, a higher selectivity, and Nernstian behavior.[140] Ionophore f contains multiple $-NO_2$ groups, which increase the compound's hydrogen bond donor capacity and its bonding affinity with CO_3^{2-} through the mechanism displayed in Fig. 3c. Similar trends in more successful carbonate ionophores based on hydrazides containing $-NO_2$ groups have been reported. (*E*)-2-(2-(4-Nitrobenzylidene) hydrazinyl)pyridine, also referred to as PDZ-1, yielded optimal results for Thimaradka and co-workers where its detection limit and limit of quantification for carbonate were 0.11 mM and 0.36 mM, respectively.[141] The structural design of PDZ-1 causes its –NH functionality to be more acidic due to an adjacent pyridine moiety and $-NO_2$ functionality in the *para*-position. These structural characteristics contribute to a more effective binding site for CO_3^{2-}. The mechanism by which PDZ-1 can bond with carbonate in a 2 : 1 stoichiometric manner is depicted in Fig. 7a. Similar to PDZ-1, ionophores labeled as R1 and R2 by Singh and co-workers also bind carbonate through a 2 : 1 stoichiometric ratio while exhibiting a high selectivity for carbonate over competing salts with a detection limit of 0.51 ppm and 0.47 ppm, respectively.[142] Structurally, R1 and R2 are similar to PDZ-1. However, they feature different heterocyclic rings containing oxygen or sulfur along with a $-NO_2$ group attached.[142] These ionophores also rely on the nitro group leading to an increased acidity of the hydrogen atom on the –NH group to elevate the compound's hydrogen bond donor capacity and selectivity for carbonate. The mechanism of carbonate binding to R1 and R2 is shown in Fig. 7b and c, respectively.

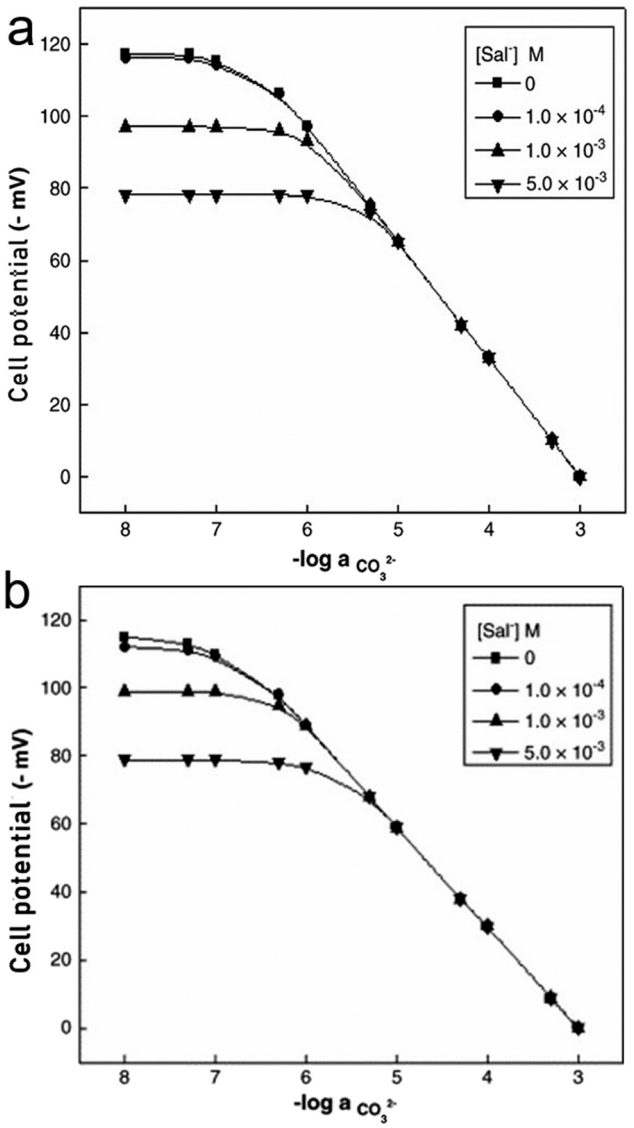

Fig. 6 Variation of cell potential of sensor based on ionophore e (a) and ionophore f (b) with activity of CO_3^{2-} at different concentration levels of Sal^- ions. Reprinted from *Electrochimica Acta*, Copyright (2006), with permission from Elsevier.[140]

5.1.2 Tweezer-type carbonate ionophores. The tweezer-type ionophore, composed of a molecular frame and ion-selective binding groups, is another promising ionophore family. These ion-selective binding groups can act as a "tweezer", trapping the target ion by binding with it at two sites. Early

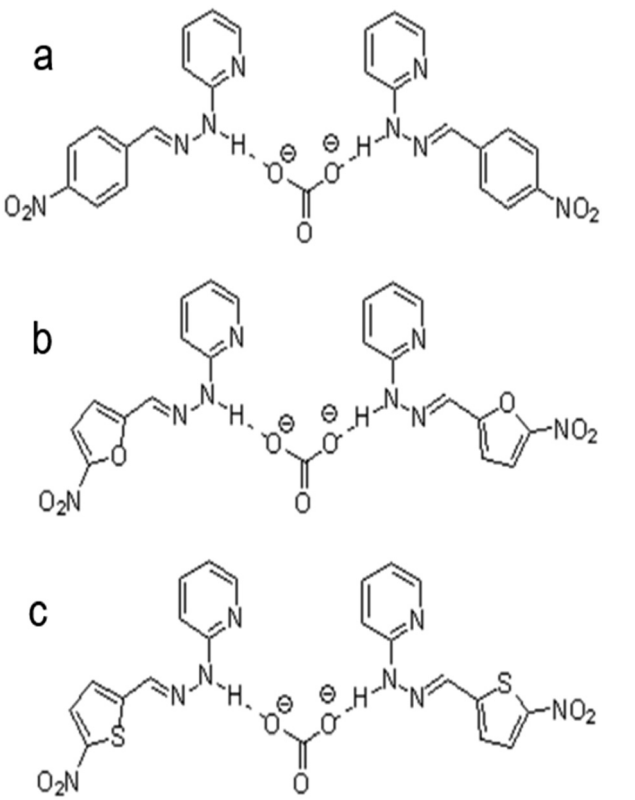

Fig. 7 Interaction mechanism between ionophore and carbonate ion: (a) (*E*)-2-(2-(4-nitrobenzylidene)hydrazinyl)pyridine (labeled as PDZ-1 by Thimaradka *et al.*), (b) (*E*)-2-(2-(5-nitrofuranylidene)hydrazinyl)pyridine (labeled as R1 by Singh *et al.*), and (c) (*E*)-2-(2-(5-nitrothiophenylidene) hydrazinyl)pyridine (labeled as R2 by Singh *et al.*).[142]

examples of this ionophore type came from Pyun and co-workers when they first reported a deoxycholic acid derivative with two trifluoroacetylbenzoyl (TFAB) moieties attached.[143] Later, Pyun and co-workers investigated numerous cholic acid derivatives bonded with 1 to 3 TFAB moieties as carbonate ionophores.[144] Results indicated a cholic acid-based ionophore with two or three TFAB moieties bound carbonate at a much greater occurrence than those with just one TFAB moiety attached. However, it was unconfirmed whether a carbonate ion could connect with two TFAB groups simultaneously.[144] Further research has determined that cholic acid derivatives with two TFAB groups attached yield the best carbonate selectivity, but the placement of these groups on the cholic acid backbone has caused some speculation.

Multiple papers reported that the best carbonate selectivity occurred when the TFAB groups had a greater distance between them than the predicted optimal distance. From the covalent bond mechanism suggested by Meyerhoff and co-workers (Fig. 3a), the optimal distance is deemed to be 4.8 Å.[135,144] However, research has detailed that longer than 7.3 Å or exactly 6 Å led to effective ionophore performance and resulted in modifications to the proposed mechanisms of carbonate binding.[145,146] Shim and co-workers have specifically detailed that ionophores with TFAB groups placed in the C3 and C12 positions displayed the best carbonate selectivity and suggest that a water molecule is also involved in the mechanism, meaning that a covalent bond with a carbonyl carbon on TFAB and a hydrogen bond with a water molecule provide the tweezer binding sites for incoming carbonates.[146] These conclusions differ significantly from that of Lee and co-workers, who propose carbonate was binding covalently to a TFAB carbonyl carbon while also binding to the hydroxyl group of cholic acid through hydrogen bonding.[145] However, in either mechanism, the greater distance between the two TFAB moieties could allow for a better conformational match.[145] With the hydroxyl groups of cholic acid in fixed spatial positions, the TFAB groups can maintain a favorable conformational structure and provide binding sites for carbonate *via* covalent and hydrogen bonds.

Further investigation of cholic and deoxycholic acid-based ionophores by Choi and co-workers using trifluoroacetyl-*p*-decylbenzene (TFADB), *N*,*N*-dioctyl-7α-acetoxy-3α,12α-bis(4-trifluoroacetylbenzoxy)-5β-cholan-24-amide (3,12-bis(TFAB) CA), and *N*,*N*-dioctyl-3α,12α-bis(4-trifluoroacetylbenzoxy)-5β-cholan-24-amide (deoxy-3,12-bis(TFAB)CA) displayed that deoxy-3,12-bis(TFAB)CA had the strongest carbonate selectivity with a greater distinction in selectivity to other anions as compared to the other two ionophores tested

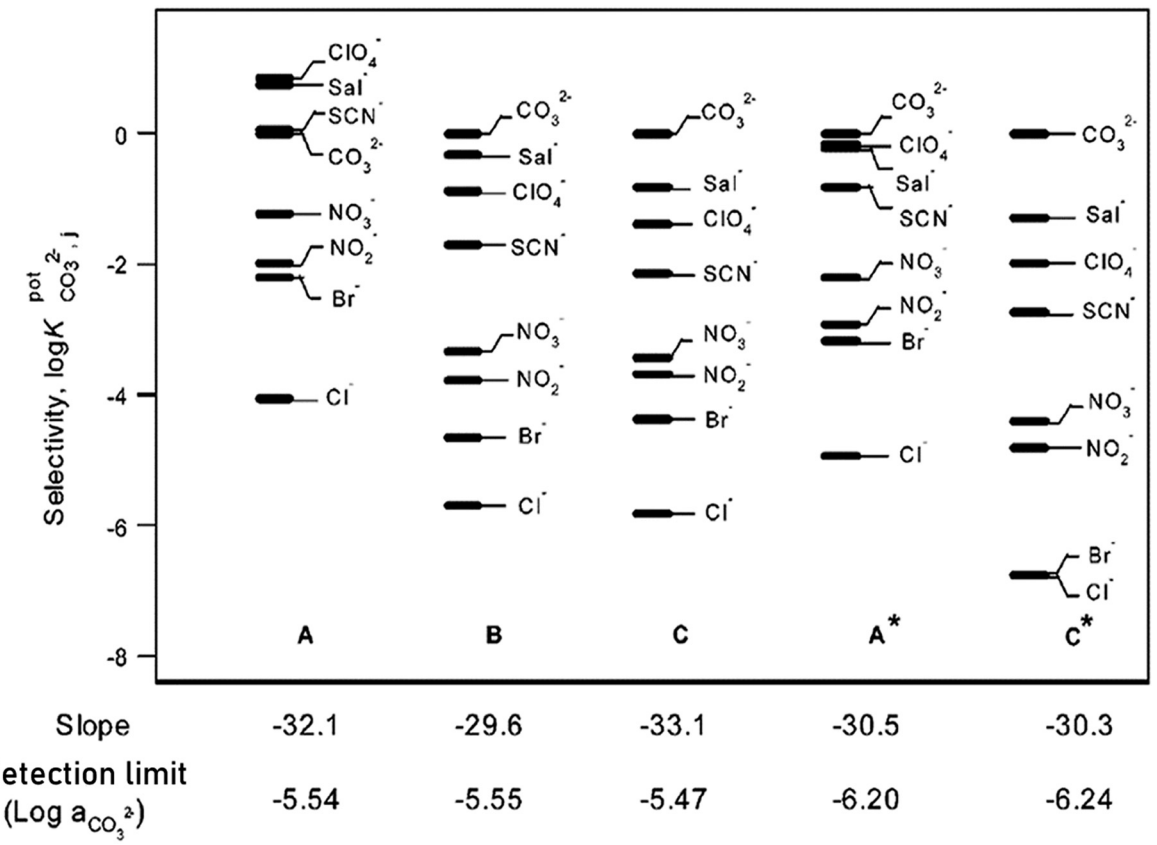

Fig. 8 The carbonate selectivity coefficients, response slopes, and detection limits of the three electrodes prepared. Electrode A using TFADB, electrode B using 3,12-bis(TFAB)CA, and electrode C using deoxy-3,12-bis(TFAB)CA. A* and C* indicate the result was obtained at a pH of 8.0. Reprinted (adapted) with permission from ref. 58. Copyright 2002 American Chemical Society.

(Fig. 8).[58] Testing in artificial seawater samples along with a wide range of carbonate selectivity has led researchers to conclude that deoxy-3,12-bis(TFAB)CA would be sufficient for seawater carbonate sensing applications.[58,147] Due to the success of this specific ionophore over time, it is now coined as the commercial carbonate ionophore VII (Fig. 8) and has been tested in a variety of conditions, including within microsensors and with ion-to-electron redox probes through anion transfer voltammetry.[119,148–150] After adjustments to ionophore quantity (16.6 mg to 16.0 mg), de Beer and co-workers found their microsensor exhibited similar interference levels to macrosensors that utilized the given ionophore and that it was sensitive to sulfide since the addition of 0.1 mol m^{-3} sulfide to a calibration solution caused carbonate selectivity to be lost.[148] This sulfide sensitivity limits its usefulness near sediment covered with seawater; however, Xie and Bakker noted that hydrogen sulfide (HS^-), a common form of sulfide, was not an interferent for their sensor composed of a carbonate selective ISE using carbonate ionophore VII and a pH electrode.[57] It is important to note that sulfide does not exist in most oxygenated oceanic environments, which suggests that a sensor using carbonate ionophore VII is applicable for marine testing. The mechanism by which carbonate ionophore VII and carbonate bind is shown in Fig. 9.

As previously indicated, carbonate ionophore VII with anion transfer voltammetry for carbonate detection has been examined. Using river samples and various cationic [6] helicenes as ion-to-electron transducers in redox probes, it was determined that cationic [6]helicene diaza embedded with two bromine groups (Fig. 10d) was the best candidate for anion transfer through the thin sensing films compared to the other helicenes tested (Fig. 10).[150] Upon progressive addition of carbonate to the sample, Nernstian peak shift behavior occurred (Fig. 11), displaying adequate performance for carbonate detection while being comparable to standard carbonate-selective electrodes that do not use redox probes at environmental pH.[150] Even though it was only tested in river water samples, it did not display any interference in the environmental pH range, which means this assembly using ion-to-electron redox probes has potential for oceanic samples in similar pH ranges.

In summary, tweezer-type ionophores have displayed highly improved carbonate selectivity due to their ability to capture carbonate between two ion binding groups, commonly TFAB groups. A deoxycholic acid molecular base has been a fundamental component of previous ionophore design due to the steroidal backbone of cholic acid. Its base contains an adequate amount of rigidness to hold the binding groups and carbonate, while not restricting the

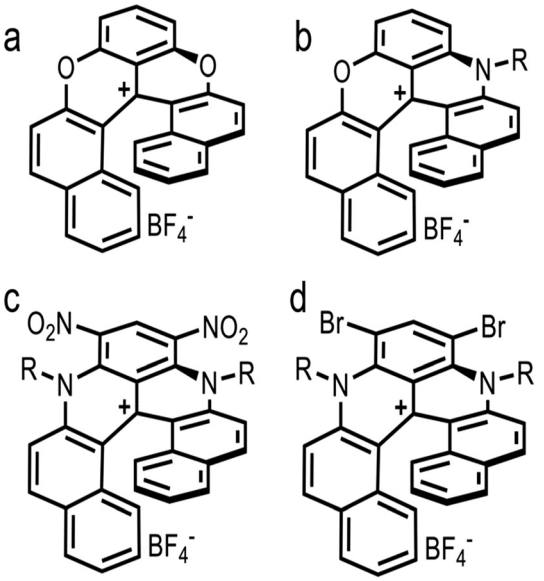

Fig. 10 Structure of cationic [6]helicene. Dioxa$^+$ (a), Azaoxz$^+C_{12}$: R = $-C_{12}H_{25}$ (b), Diaza$^+(C_8)_2(NO_2)_2$: R = $-C_8H_{17}$ (c), and Diaza$^+(C_8)_2Br_2$: R = $-C_8H_{17}$ (d).

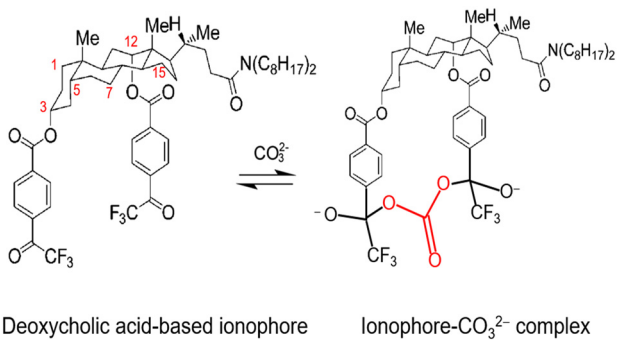

Fig. 9 Mechanism between a deoxycholic acid-based ionophore (commercial carbonate ionophore VII, *N,N*-dioctyl-3α,12α-bis(4-trifluoroacetylbenzoxy)-5β-cholan-24-amide, or deoxy-3,12-bis(TFAB) CA) and carbonate, which results in an ionophore-carbonate complex. Here carbons on deoxycholic acid fragment are selectively labeled to show the positions of the TFAB functionality.

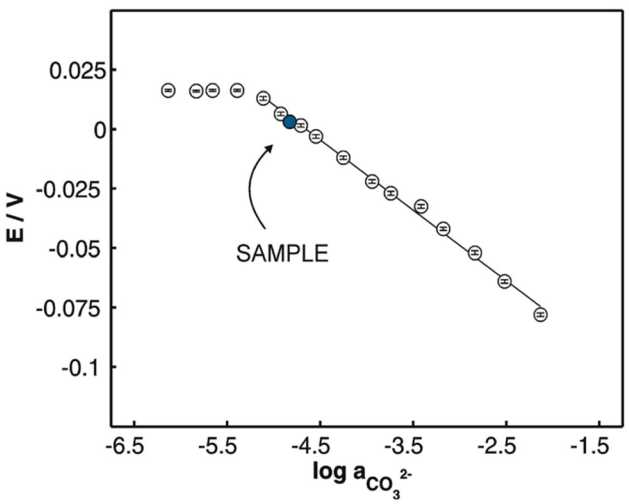

Fig. 11 Observed Nernstian shift for progressive carbonate additions (MA14) in a sample containing a pH of 8.20 through the addition of 0.2 mM NaCl. Reprinted with permission from ref. 150. Copyright 2018 John Wiley and Sons.

interactions. Furthermore, the locations of the potential binding sites lie on the same side of the molecule, which prevents complications regarding conformation. Thus, ionophores with a deoxycholic base bearing two TFAB groups will remain a contender in future research of carbonate detection.

5.1.3 Metal-based complexes as carbonate ionophores. Although tweezer-type ionophores, especially carbonate ionophore VII, are the most promising candidate for carbonate detection, metal-based complexes have also been investigated recently. For instance, three fluorophilic salen derivative based manganese(III) complexes resulted in enhanced CO_3^{2-} selectivity compared to previously reported ISEs, with interference from Cl^- and Sal^- being reduced by 2 and 6 orders of magnitude, respectively.[151] The structures of the ionophores (labeled as Mn-1, Mn-2, and Mn-3 by the authors from the original paper) are in Fig. 12. The CO_3^{2-} selectivity for each ionophore was tested while altering the ionic sites to ionophore molar ratio. Comparing the three complexes, Mn-1 and Mn-2 exhibited stronger CO_3^{2-} selectivity than Mn-3. Both Mn-1 and Mn-2 had adequate selectivity for CO_3^{2-} with an anionic site-to-ionophore molar ratio of 1 : 4. However, Mn-2 exhibited a higher CO_3^{2-} selectivity in these conditions. The slight difference in performance seems to occur because the structure of Mn-2 causes less steric hindrance, allowing the formation of 2 : 1 complexes. The steric hindrance present in the structure of Mn-1 favors 1 : 1 complexes and allows the ionophore to perform more optimally with a 2 : 3 cationic site-to-ionophore ratio.[151] As demonstrated with tweezer-type ionophores, the formation of 2 : 1 complexes between a given ionophore and carbonate is advantageous compared to others. Therefore, metal-based complex ionophores like Mn-2 should be further explored with seawater samples to determine their efficacy for ocean acidification research.

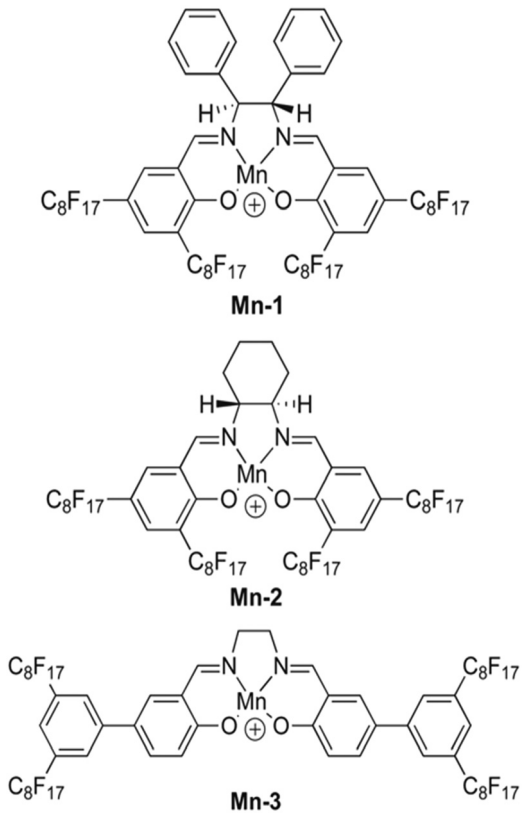

Fig. 12 Structure of fluorophilic manganese(III) complexes, labeled as Mn-1, Mn-2, and Mn-3.[151]

6. Ion-selective membrane fabrication

While the ionophore is crucial to the analyte binding capability of a sensor, other components within the ion-selective membrane also affect the performance and properties of the device (*e.g.*, measuring range, selectivity, sensitivity, response time, stability, and reproducibility). Thus, these membrane components must be chosen carefully to ensure the functionality of the sensor in its target environment. Various types of membranes, including glass, crystalline/solid-state, liquid, and polymeric membranes, have been studied for ISE preparations. Conventionally, liquid membranes have been a part of ISEs; however, more recent developments commented on the difficulties of this membrane type.[152–154] Hence, polymeric membranes have become common for carbonate electrochemical sensors. They typically consist of a polymer or copolymer as a substrate, an ionophore, and ionic additives. However, with a polymer as a substrate, a plasticizer may also be added to the composition to adjust the mechanical property of the resultant membranes.[155] Historically, the general breakdown of membranes that include plasticizer has been 1% ionophore, 33% poly(vinyl chloride) (PVC), and 66% plasticizer by mass.[156] Over time, various combinations of these components with ionic additives have been tested and optimized to understand how each constituent affects the function of the membrane. Currently, the optimized composition of a membrane with PVC as the polymer substrate contains 33% PVC, 65% plasticizer, 2% ionophore, and 60 mol% additive relative to the ionophore.[157]

The early addition of polymer, whether it was silicone rubber or PVC, led researchers to believe that polymers could provide elasticity and mechanical stability to the membrane.[158–160] However, more recent research by Zhao and Cai has demonstrated that a polymer affects the adhesive properties (*i.e.*, how well it attaches to the electrode body) and the mechanical strength of the membrane (*i.e.*, how long the membrane can remain intact while undergoing biofouling), which both impact the lifetime of the sensor.[161] Besides PVC, some other materials used for ion-selective membranes include silicone, polyurethane, and carboxylated PVC.[159,162,163] Independent of the polymer, a solvent is required to stimulate the dissolution of the polymer substrate. Frequently, tetrahydrofuran (THF, bp 66 °C) is used as a solvent to dissolve the polymer; however, other commonly used solvents include dimethylformamide (DMF, bp 153 °C), *N*-methyl-2-pyrrolidone

(NMP, bp 202.0 °C), dimethylacetamide (DMAc, bp 165 °C), and dimethyl sulfoxide (DMSO, bp 189 °C).[57,58,86,111,119,123,136,138,140,145,148,161,164–168] These solvents are later evaporated out of the solution within the membrane preparation process.

Sensor lifetime is also dependent on the rates of diffusion of the ionophore and plasticizer in the membrane.[169,170] Plasticizers have two main purposes within a polymeric membrane, which are to provide elasticity or fluidity and to act as a co-solvent for the ionophore.[152] The chosen plasticizer must be compatible with the polymer substrate so it may encourage the high mobility of the other components in the membrane (*i.e.*, the ionophore).[160] The mobility of the ionophore, along with the identity and characteristics of the ionophore, influences sensor selectivity. Some examples of plasticizers in ion-selective membranes are dioctyl adipate (DOA), 2-nitrophenyl octyl ether (*o*-NOPE), dioctyl sebacate (DOS), dioctyl phthalate (DOP), bis(2-ethylhexyl)adipate (DEHA), tris(2-ethylhexyl)phosphate (TEHP), 1-chloronapthalene (CN), and diethyl phthalate (DEP).[57,58,86,119,124,133,136,140,145–147,161,166,167] Generally, more plasticizer corresponds to greatly improved physical properties, higher flexibility, and higher ionic mobility.[145] As a result, most membranes contain a higher amount of plasticizer than polymer substrate. Overall, the percentage of polymer should be limited to avoid complications with solubility; however, enough polymer should be present to support the adhesive and mechanical properties of the membrane.

In addition to the ionophore and its mobility, the concentration of other active sensing components, such as ion exchangers or ionic additives, in the membrane affects sensor selectivity.[171] Previously, research showed that low amounts of ion exchangers or ionic additives would create the most effective membranes; however, newly developed neutral ionophores require ionic additives to preserve the membrane's composition.[152,165] Furthermore, these additives can improve the permselectivity of neutral ionophores. Improvements in sensor selectivity have also been documented in sensors with charged ionophores and ionic additives in the membrane.[172–178] Hence, ionic additives or ion exchangers can improve selectivity regardless of the selected ionophore. Research has shown that additives improve selectivity by reducing interference from the other ions a sensor may encounter.[179] However, an optimal additive to ionophore molar ratio must be used to obtain these improvements.[94] The current optimal additive to ionophore ratio is reported to be 60 mol% additive to ionophore.[157] Improved selectivity positively impacts the reproducibility and lifetime of the sensor.[180] Therefore, a key component for designing ISEs with a high selectivity is limiting or eliminating ionic impurities in the membrane so the ionic additives can function optimally within the membrane.[165] Some examples of ionic additives used within polymeric membranes are methyltridodecylammonium chloride (MTDDACl), tridodecylmethylammonium chloride (TDMACl or TDDMACl), and potassium tetrakis(*p*-chlorophenyl)borate (KT*p*ClPB).[57,58,119,124,136,138,140,145–148]

Various techniques exist for preparing polymeric membranes based on desired morphology, geometry, mechanical strength, and function. These membranes can be isotropic (*e.g.*, nonporous dense membranes, microporous membranes, and electrically charged membranes) or anisotropic (*e.g.*, integrated asymmetric membranes, composite membranes, and supported liquid membranes), which require different fabrication processes.[181] A detailed discussion of various fabrication processes (*e.g.*, extrusion, phase inversion, diffusion induced phase separation, and others) does not lie within the scope of this review, but has been reported in detail.[182,183] The casting method is often used for membrane preparation for carbonate detection. This method normally involves the formation of a cocktail solution, or mixture of membrane constituents; however, the components included in this initial mixture vary.[160] In most cases, the polymer, ionophore, plasticizer, and ionic additive are mixed and dissolved in solvent, resulting in an uniform solution before casting.[57,58,124,136,138,140,145,146] However, in some cases, the ionophore, plasticizer, and ionic additive are dissolved in the solvent before the polymer substrate is mixed in.[134] In either procedure, the resultant homogeneous mixture is poured onto a glass ring on a glass surface where it can be left for some time to evaporate the solvent slowly. Previously reported evaporation time lengths for THF include 24 hours, 48 hours, and overnight.[57,58,124,133,136,138,140,145,146] After the solvent has evaporated, the desired membrane disks are punched out from the cast membrane and mounted onto the electrode body. This process contains modifications for microsensors or solid-state sensors.[119,147,148]

7. Evaluating a potentiometric electrochemical sensor

Evaluating a potentiometric electrochemical sensor requires the determination of various properties, including sensitivity, measuring range, selectivity, response time, and lifetime. As discussed in section 6, all components of the ion-selective membrane impact these properties, which control the functionality of the sensor. Ideally, measuring all properties results in the most precise evaluation of a sensor; however, publications usually only measure and report a few of these properties. The reported performance of carbonate electrochemical sensors using carbonate ionophores is listed in Table 1.

7.1 Sensitivity, detection limit, and measuring range

As described in section 4.2.2, the potentiometric response of a sensor should follow the Nernst equation (eqn (5)) and have an experimental response slope close or equal to −29.6 mV per decade or 59.2 mV/*z*. A calibration curve can be plotted with the line of best fit to determine the experimental response slope of the linear section of the curve. The slope of

Table 1 Reported performance of carbonate sensors

Carbonate ionophore	Testing media	Measuring range	Sensitivity	Response time	Lifetime	Ref.
Trifluoroacetyl-*p*-butylbenzene	Water & 0.1 M NaCl solution	10^{-7}–10^{-2} M	Near Nernstian	30 s–2 min	—	121
p-Butyl-α,α,α-trifluoroacetophenone, *p*-decyl-α,α,α-trifluoroacetophenone	Hospital patient samples	—	20–25 mV per decade	—	1 week	111
BTFAB, HDTFAB, & DDTFAB	Bovine serum	Reached linearity	−29.9–−14.1 mV per decade	—	—	138
3,7-Bis(TFAB)CA, 3,12-bis(TFAB)CA, & 7,12-bis(TFAB)CA	Diluted serum	—	−29.6–−18.5 mV per decade	—	—	145
3,12-Bis(TFAB)CA, deoxy-3,12-bis(TFAB)CA, & TFADB	Artificial seawater	—	−33.1–−29.6 mV per decade	—	—	58
TFAP-CA	Artificial gradients	—	27–30 mV per 10-fold concentration change	60 s	3–5 days	148
Mn-1, Mn-2, & Mn-3	Treated water & $NaHCO_3$	—	Close to −29.6 mV	Few s	—	151
Carbonate ionophore VII	Freshwater aquarium	—	—	5 s	—	57
Deoxy-3,12-bis(TFAB)CA	Seawater & marine sediment	2–300 μmol kg^{-1}	28–31 mV	—	5–7 days	119
3,12-BisTFAB with *N*,*N*-dioctyl-3α,12α-bis (4-trifluoroacetylbenzyloxy)-5-cholan-24-amide	Standard solutions with 0.05 M Tris-H_2SO_4 (pH 8)	Limit of 2 × 10^{-4} M	−29.5–−29.2 mV per decade	—	2 weeks	147
Hex-TFA, NO_2-TFA, & Br-TFA	0.1 M of sodium salts & Tris 0.01 M + H_2SO_4 (pH 8.5)	Limit of 7 × 10^{-7} M	29 ± 1.5 mV per decade	—	—	136
3-Bromo-4-hexyl-5-nitrofluoroacetophenone	0.1 M of interfering anions & sodium salts with Tris 0.01 M + H_2SO_4 (pH 8.5)	—	92–121 mV dec^{-1} −48.1–−30.1 mV pH^{-1}	—	—	124
Substituted cholic and deoxycholic acid derivatives	Artificial & real seawater	—	−63.3–52.9 mV per decade	—	—	146
N,*N*^{1}-Bis(phenyl)isophthalohydrazide & *N*,*N*^{1}-bis(2,4-dinitrophenyl) isophthalohydrazide	Tris 0.01 M + H_2SO_4 & varying $NaHCO_3$ concentrations (pH 8.6)	1.3 × 10^{-7}–1 × 10^{-3} M	28–32 mV per decade	7–50 s	2½ months	140
Carbonate ionophore VII	Arve river, Geneva	2.3 μM–1 mM	27.2 ± 0.8 mV per decade	1 s	—	197
N,*N*^{1}-Bis(2,4-dinitrophenyl) isophthalohydrazide	Artificial seawater	Limit of 5 ppt	Near Nernstian	—	—	29
Carbonate ionophore VII	Outdoor mesocosm & Genoa harbor	10^{-5}–10^{-1} M	−27.8 mV per decade	<10 s	3 weeks	31
Carbonate ionophore VII	Seawater	10^{-5}–10^{-1} M	−30.4 mV per decade	<1 s	>60 days	98

the linear section of the curve represents the sensitivity of the sensor by describing how its measurements fluctuate per change of analyte concentration in the sample. Ideally, it should be close or equal to Nernst slope to indicate optimal sensitivity.[98] Evaluating the experimental response slope can also verify whether the intended target analyte is being measured. Research reports that response slopes around −30 mV per decade indicate response to carbonate, whereas slopes around −60 mV per decade indicate response to bicarbonate.[35] In the past, unusually high Nernst slopes (*i.e.*, super-Nernstian slopes) were attributed to transmembrane ion fluxes or the presence of primary and interfering ions in the ion-selective membrane.[103,184–191] However, more recently, research suggests that super-Nernstian slopes may occur when the ionophore and target ion simultaneously form different stoichiometric complexes (*e.g.*, 1:1 and 2:1 complexes) or when there is an excessive inward concentration gradient.[99,192] Based on these new findings, researchers should carefully evaluate their device if super-Nernstian slopes are observed. If the sensor's sensitivity needs improvement, an effective process for improving sensor sensitivity is the activation of the membrane before sensor use, which is known as aging the membrane.[193] Recently, improved sensitivity from aged membranes was demonstrated in carbonate microsensors by Han and co-workers. In their experiments, the carbonate electrodes were aged through submersion in an electrolyte before calibration and testing. The carbonate electrode aged in the electrolyte for 24 hours exhibited a sensitivity closer to the Nernst slope than the electrode submerged for only 8 hours.[119] This improvement in sensitivity may be attributed to the change in potential that resulted from an equilibrium established between the inner and outer sides of the membrane when aged.

Along with the sensitivity, the detection limit and measuring range of a sensor can be determined using the calibration curve. The detection limit is the lowest concentration that can be measured while differing from a measurement obtained from a blank sample.[194] Using a calibration curve, measurements from a blank sample, and

extrapolation, the equation of best fit can reveal the detection limit.[195] For ocean acidification research, carbonate ion concentrations in some oceanic and estuarine waters may vary between 30 to 300 μmol kg^{-1}, so a detection limit as low as a few μmol L^{-1} (10^{-6} M) will be ideal. Sokalski and co-workers reported that the improvement in the lower detection limit of a sensor could be achieved with an internal solution containing a high concentration of an interfering ion with a low concentration of the target ion.[196]

Similar to sensor sensitivity, the measuring range is determined from the domain of linearity. Within this domain, the analyte concentrations encountered by the sensor represent the analyte concentration range that can be reliably measured since the sensor is operating with Nernstian behavior. Jain and co-workers plotted Fig. 13 to determine the sensitivity, detection limit, and measuring range for six of their sensors, which they labeled as sensors 7–12. Each of their sensors contained a PVC membrane with varying plasticizers. The membrane of sensor 7 contained no plasticizer, while the membranes of sensors 8–12 contained TEHP, DOS, DOP, CN, and DEP, respectively. Sensor 11 produced the greatest range of linearity, resulting in a detection limit of 1.3×10^{-7} M and a measuring range of 1.3×10^{-7} to 1.0×10^{-2} M while maintaining Nernstian behavior (29.0 mV per decade).[140] Song and co-workers produced a similar figure (Fig. 14) to display sensitivity and detection limit. From Fig. 14, the slope and detection limit for electrodes a, b, and c were −29.3, −29.2, and −29.5 mV per decade and 2.0×10^{-4}, 2.6×10^{-4}, and 2.7×10^{-4} mol L^{-1}, respectively.[14] To date, multiple carbonate sensors have demonstrated near Nernstian and Nernstian behavior

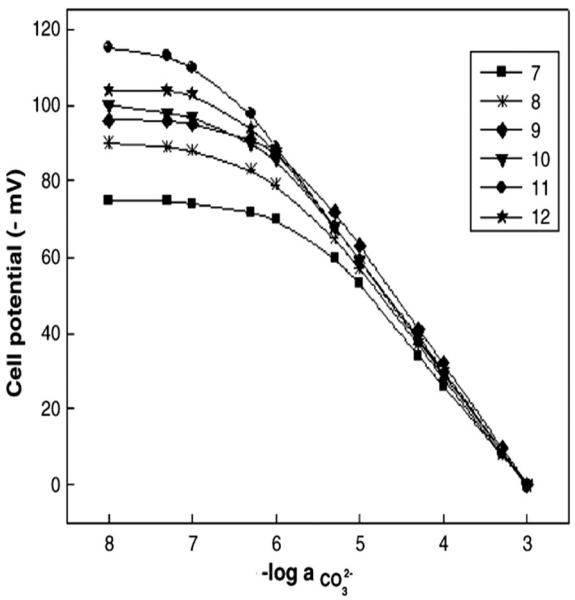

Fig. 13 Calibration curves produced by sensors 7–12 from Jain *et al.* The membranes were PVC based without plasticizer (7) and with the plasticizers of TEHP (8), DOS (9), DOP (10), CN (11), and DEP (12). Reprinted from *Electrochimica Acta*, Copyright (2006), with permission from Elsevier.[140]

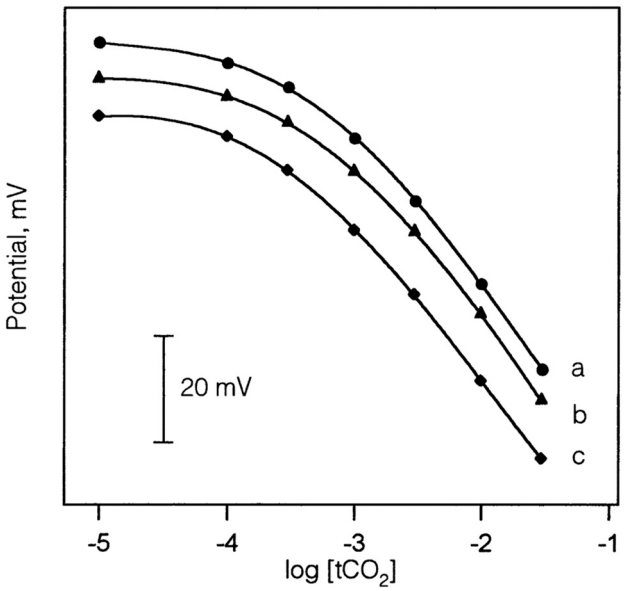

Fig. 14 Calibration curves of sensors with an Ag/AgCl (a), a PHDP-modified Ag/AgCl (b), and a POT-modified Ag/AgCl electrode (c) produced by Song *et al.* All three sensors exhibited Nernst behavior and a similar detection limit of 2.0×10^{-4} M. Reprinted from *Talanta*, Copyright (2002), with permission from Elsevier.[147]

(Table 1). Almost all publications listed in Table 1 reported the sensitivity of their device. The detection limit, however, has not been consistently reported. The lowest detection limit of the sensors in Table 1 was reported by Makarychev and co-workers (2003) as 7.0×10^{-7} M.[136] Like the detection limit, the measuring range of sensors is not as frequently reported as the sensitivity, but it is reported more often than the detection limit. For sensors tested with appropriate ion solutions, Herman and Rechnitz reported the widest measuring range of 10^{-7} to 10^{-2} M.[121] Jain and co-workers reported a similar range of 1.3×10^{-7} to 1.0×10^{-3} M.[140] For sensors tested in seawater or river water samples, reported measuring ranges include 2 to 300 μmol kg^{-1}, 2.3 μM to 1 mM, and 10^{-5} to 10^{-1} M.[65,99,119,197]

7.2 Selectivity

Selectivity is the property of ISEs that allows them to be useful for detecting target ions from a complicated matrix or environment of multiple ions. Many definitions exist, but the accepted IUPAC definition explains selectivity as a measure of how well a method can distinguish and quantify a particular analyte in the presence of interferents.[198]

In seawater, the common interferents for carbonate include Cl^-, Sal^-, SCN^-, NO_3^-, NO_2^-, Br^-, SO_4^{2-}, and HPO_4^{2-}.[58,126] As a result, the selectivity of a sensor for these ions and carbonate are compared to evaluate the sensor's ability to target carbonate. Usually, ISEs respond to anions according to the Hofmeister series.[199] Because carbonate and bicarbonate are highly hydrophilic and fall on one end of the series ($CO_3^{2-} > SO_4^{2-} > S_2O_3^{2-} > H_2PO_4^- > F^- > Cl^- > Br^- >$

$NO_3^- > I^- > ClO_4^- > SCN^-$), developing electrodes with high selectivity for them is challenging. Furthermore, the challenge becomes more profound if the electrode is intended for use in an environment with a high chloride concentration, such as seawater. The chloride level in seawater is about 0.5 M, while the level of bicarbonate/carbonate is only around 0.002 M. Therefore, the required selectivity to measure bicarbonate/carbonate in a 250-fold chloride environment should be 4×10^{-5} based on calculation.

Various techniques exist for measuring selectivity coefficients. Methods are typically categorized as either a mixed solution method or separate solution method.[200] An in-depth discussion of each method does not fall within the scope of this review, but extensive detail has been reported elsewhere.[200–203] Some examples of methods used in ocean acidification research include the separate solution method (Fig. 5) and the matched potential method (Fig. 8).[58,126]

As discussed in section 6, the selectivity of a sensor is greatly influenced by the membrane composition. The addition of plasticizer, which is critical for the mechanical properties of the membrane and the mobility of the ionophore, can improve selectivity. If the ionophore is electrically charged, an optimized ratio of ionophore and ionic sites in the sensing membrane is predicted to provide the highest selectivity. Furthermore, adding ionic sites with the same charge as interfering ions can also improve selectivity.[195] To ensure the measured selectivity is accurate, the sensor should be evaluated for the presence of a gas leak, especially for CO_2 diffusion in or out of the test setup. If a gas leak occurs, the error will be magnified on calibration curves once the carbonate concentration approaches 1×10^{-6} M.

7.3 Response time

The response time of a sensor is how quickly a sensor can produce a readable signal after exposure to an analyte.[204] In their guidelines, IUPAC describes the dipping and injection methods as techniques for determining the response time of a sensor.[205] For microsensors, Merikhi and co-workers describe the jet-nozzle method.[204] Regardless of the method, it is ideal to test the sensor in field conditions (*e.g.*, seawater) or similar conditions (*e.g.*, artificial seawater or various solutions containing the target analyte and interferents) for an accurate response time.[204] For example, Jain and co-workers measured the response time of their carbonate sensor using solutions containing CO_3^{2-}.[140] Initially, they exposed their sensor to a solution containing 1.0×10^{-5} M of CO_3^{2-}. After the sensor stabilized in this solution, Jain and co-workers increased the $[CO_3^{2-}]$ to 1.0×10^{-4} M and measured the time it took the sensor to stabilize in the new solution as the response time. In their experiments, they tested 12 carbonate sensors with varying membrane compositions, analyzing two carbonate ionophores displayed in Fig. 4e and f and four plasticizers (TEHP, DOS, DOP, CN, and DEP). The sensor containing the ionophore f and the plasticizer CN demonstrated the lowest response time of 7 seconds. In their sensors containing ionophore e, the sensor membrane also containing CN performed the best with a response time of 10 seconds.

For ocean acidification research, a short response time is vital to ensure that small, frequent changes in carbonate concentration are captured. As an example, Yuan and co-workers determined the response time of their sensor to be 1 second by adding successive additions of bicarbonate to 0.1 M Tris-H_2SO_4 buffer solution and monitoring the time until the sensor produced a stable potential after each addition (Fig. 15).[197] Because this sensor was tested in field conditions (Arve river), it displays great promise for ocean acidification research. Another carbonate sensor built by Zhang and co-workers displayed an excellent response time of less than 1 second through the immersion method.[98] At the time of this publication, this response time is the best reported for carbonate sensors to the best of our knowledge. The reported response times for multiple carbonate sensors can be found in Table 1. Some other notable response times include less than 10 seconds while operating in an outdoor mesocosm and in the Genoa Harbor and 60 seconds while operating in artificial gradients in agar, freshwater tufas, foraminifera, and microbial mats.[32,148]

The response time of a sensor is related to the size and thickness of its sensing membrane. Generally, increasing the contact area between the test solution and the film and reducing the thickness of the membrane can improve the response speed of the electrode. A membrane that is too thick leads to larger resistance and will not properly

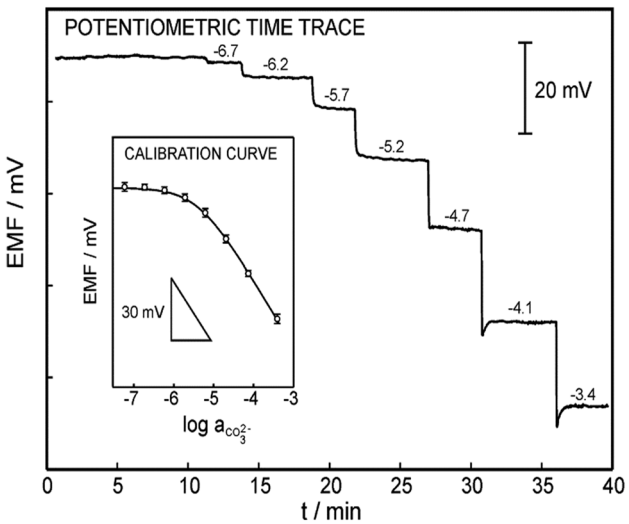

Fig. 15 Analytical performance of the carbonate electrode made by Yuan *et al.* The response time was obtained by adding successive additions of bicarbonate to 0.1 M Tris-H_2SO_4 buffer (pH = 8.6). Inset: A triplicate of the calibration curve (RSD = 1.5%) as a function of the carbonate activity (slope = −27.2 ± 0.8 mV per decade, LOD = 2.3 μM). Reprinted (adapted) with permission from ref. 197. Copyright 2015 American Chemical Society.

facilitate electron transfer, resulting in a longer response time. The sensor lifetime is another important parameter which could be influenced by the thickness of the film (discussed in the next section). According to the environment where the sensor will be used, a balance should be made between the lifetime and response time when designing the membrane.

7.4 Lifetime

The lifetime, or how long a sensor can operate at a functional capacity, is affected by many factors. As previously mentioned, biofouling, the composition of the membrane, and size and thickness of the membrane affect the lifetime of sensors. Moreover, based on previous investigations by Sun and co-workers, proper activation of the membrane (*i.e.*, aging) in a buffer solution is necessary for a newly prepared electrode to reach a relatively slow potential drift rate and respond effectively to target ions over time.[206] Storing the device in a dry environment and avoiding strong redox active species could also be a good way to slow down the potential decrease and prolong the working life.[206] Throughout the literature, lifetimes have been reported from three days to two and a half months for carbonate sensors (Table 1).[140,148] On average, the lifetime of ISEs, including those not involved in ocean acidification research, is from 4 to 10 weeks.[160] Commonly, the sensitivity of a sensor is measured at least once every week to confirm if the sensor is continuing to operate effectively.[161] Zhao and Cai reported that once the sensitivity fell below 52 mV pH^{-1}, the lifetime could be determined.[161] However, Jain and co-workers used reproducible potential and a low standard deviation of 0.3 mV to determine a lifetime of two and a half months.[140]

Lifetime is an important parameter, especially for liquid microelectrodes. Fabricating thin and large-diameter liquid-membraned microelectrodes facilitates fast response. However, such thin membranes are more susceptible to change because of gradual leakage, which may result in a reduced lifetime. Conversely, a thick membrane with a small tip diameter could provide a longer lifetime, but may lead to high impedance, high noise, slow response time, and a slow aging process. Han and co-workers sought to determine an optimal combination of membrane thickness and diameter to balance the response time and lifetime of liquid microelectrodes. They concluded that a carbonate microelectrode membrane with a thickness and tip diameter of 100 μm and 20 μm, respectively, provided a balance with adequate tip strength and quicker membrane aging. The CO_3^{2-} microsensor fabricated to this specification can be used for 5–7 days and the drift rate can be decreased to nearly 1–2 mV h^{-1} after a stabilization period of 1 day.[119]

Overall, all properties used for evaluating an electrochemical sensor contribute to the lifetime of the device. Thus, a sensor's lifetime is the clearest indicator of a sensor's ability to function in the desired capacity.

7.5 Evaluating the connection between carbonate ionophore structure and sensor performance

In this review, three types of carbonate ionophores are discussed, including small molecules, molecular tweezers, and metal-based complexes. Each ionophore type is distinct and presents structural advantages and complications that impact sensor performance. It is necessary to note that other components of reported sensors may also boost or worsen performance. In other words, positive or poor performance cannot be solely attributed to the ionophore; however, specific structural characteristics within carbonate ionophore types may assist in enhancing carbonate detection and sensor performance.

Small organic molecules are advantageous because they can be easily modified compared to molecular tweezers and metal-based complexes. Various substituents can be attached to the phenyl ring to adjust its properties and ability to bind carbonate. For example, increased acidity and hydrogen donor capacity have increased bonding with carbonate, leading to a lower detection limit and better carbonate selectivity, lipophilicity, and sensor lifetime. Incorporating $-NO_2$ groups has been frequently credited for these enhancements.[126,134,140–142] In addition, the simultaneous presence of a –Br substituent and a $-NO_2$ group may lead to these improvements.[124] Unlike small organic molecules, molecular tweezers and metal-based complexes are challenging to develop and adjust because of conformation complications like steric hindrance. However, highly improved carbonate selectivity has been reported with molecular tweezers and metal-based complexes, especially those forming 2 : 1 complexes with carbonate.[141,142,145,146,151] The ability of molecular tweezers and metal-based complexes to bind with carbonate in two places seems to increase the reliability of carbonate detection, which small organic molecules do not currently offer. Even though all three carbonate ionophores experience some level of interference, small organic molecules tend to be more vulnerable to interferents. As a result, designing a molecular tweezer or metal-based complex ionophore with a strong base, two binding sites for carbonate, and functional groups that increase acidity and hydrogen donor capacity seems to be the most favorable ionophore structure.

8. Summary and future research

Carbonate ions are present in various clinical and environmental processes. As a result, monitoring the carbonate concentration in clinical and environmental samples is essential for advancing disease screening and environmental monitoring. In the past few decades, tracking the carbonate concentration within ocean waters has become increasingly important due to ocean acidification. Research has shown that potentiometric electrochemical sensors based on novel carbonate ionophores have the potential to be highly selective and sensitive to carbonate while remaining stable in marine environments. Carbonate ionophores have

proved to be a vital component of these devices by detecting carbonate through various mechanisms (*e.g.*, hydrogen bonding, covalent bonding, the electron-withdrawing effect, and the entrapment of the analyte). However, many challenges currently complicate the ability of these sensors to capture accurate *in situ* carbonate measurements during long-term deployment. As a result, there are several possibilities for future research in this field.

Further development of novel carbonate ionophores is anticipated. Based on the rich diversity of organic synthesis methods, ionophores with novel functionalities and structures to enhance carbonate selectivity over interfering ions are expected. At the time of this publication, a molecular tweezer or metal-based complex with a strong base and two binding sites for carbonate seems to be the most favorable carbonate ionophore structure. Multiple publications have also reported the positive effect of increased acidity and hydrogen donor capacity on carbonate selectivity. Because of this, functional groups that increase these properties must be considered and potentially added to molecular tweezers or metal-based complexes.

The issues caused by the internal reference solution must be addressed to extend the lifetime of sensors. Solid-state ISEs may overcome these issues since these devices replace the internal solution with a solid-contact transducer.[109] A conductive polymer is typically used as a solid-contact transducer to increase the sensor's stability and reduce dissolved oxygen interference.[29,109,147] Carbon nanotubes and carbon film can also be a solid-contact transducer to provide a large contact area with the ion-selective membrane, an adjustable surface, and resistance to CO_2 and O_2.[98,109] Future research must continue to evaluate these materials and others (*e.g.*, metal non-porous films) to determine which is best for sensor stability.[109]

Ocean acidification research efforts may move towards solid-state ISEs since they eliminate the internal reference solution and seem more suitable for long-term deployment. Two recent approaches using solid-state ISEs for *in situ* water monitoring include allowing direct contact between the electrodes and the water and containing the electrodes inside a fluidic-based submersible device.[207,208] The first approach, which allows direct contact between the electrode and water, is advantageous because it can provide continuous measurements and capture minute changes in analyte concentration. However, this device has only been tested in freshwater environments for a short time, so more testing is needed to determine if the device is suitable for long-term deployment in seawater. Biofouling will likely be an issue with this sensor design because of the direct contact between the electrode and water. Overall, possibilities for preventing biofouling are desperately needed in this research field. The second approach of placing solid-state ISEs within a submersible fluidic device is incredibly appealing since it has been deployed in seawater for carbonate measurement. For three weeks, the device operated optimally; however, its design did not allow for continuous measurement due to its hour-long *in situ* calibration process. The *in situ* calibration process is beneficial for reducing interference, but it prevents the sensor from capturing minute changes in carbonate concentration. Future research should investigate how to simplify the *in situ* calibration process to increase the capture of carbonate concentration.

Future research may also move towards the creation of carbonate microsensors. Microsensors are likely to have a simple design and low production costs, which makes them appealing for large-scale implementation. A reported classical potentiometric carbonate microsensor was highly selective to carbonate with a response time of 60 seconds and a lifetime of 3–5 days following a simple calibration procedure.[148] Based on these results, microsensors may require a relatively simple calibration process compared to macrosensors and be more suitable for continuous measurement. Further investigation of a reliable method for forming durable membranes of such a small radius (several micrometers) is needed. These membranes must be able to induce the diffusion process and lead to a rapid signal while remaining resistant to biofouling and pressure. Recently, a miniaturized carbonate solid-state ISE was tested in seawater, even in deep-sea conditions.[98] The sensor's design had a 0.5 mm diameter and a 6 to 12 mm length with carbonate ionophore VII and carbon film in its structure. The device was resistant to seawater interference and displayed Nernstian behavior with a response time and lifetime of less than 1 second and over 60 days, respectively. Therefore, integrating solid-state ISEs into microsensors may be even more favorable for ocean acidification research. In this design, issues from the internal reference solution would be eliminated while lowering production costs. Furthermore, carbonate microsensors could be integrated into sensor devices with other electrodes to create a device capable of simultaneously monitoring multiple oceanic parameters (*e.g.*, pH and pCO_2).

In recent studies, optodes have been tested in seawater and other natural waters.[61–64] They are reported as small and easy-to-use versatile sensors with low drift, fast response time, and long lifetime. In one study, an optode was designed with a battery that may enable deployment for over a year without required service.[63] In addition, a simple copper guard can protect these sensors against biofouling.[61] These characteristics demonstrate potential for ocean acidification research; however, these sensors have only detected dissolved oxygen, carbon dioxide, and pH. Future research could involve designing an optode for carbonate detection and testing the device in varying salinities, pressures, and temperatures.

As anthropogenic atmospheric CO_2 continues to dissolve into the ocean at increased rates, the urgency to accurately monitor ocean acidification and limit anthropogenic CO_2 emission amplifies. In the Paris Agreement, many countries committed to gradually reducing greenhouse gas emissions by 2030.[209] Recently, a new clean strategy to reduce greenhouse gas emissions by transforming atmospheric CO_2 into useable chemicals and fuels may become the driving

force towards carbon neutrality.[209–212] The large-scale implementation of ocean-based carbon dioxide removal (CDR) technologies coupled with this new promising strategy to reduce CO_2 emission has enormous potential to mitigate climate change and prevent further ocean acidification.

Author contributions

Stefanny N. Toala: investigation, conceptualization, writing – original draft, and writing – review and editing. Zhentao Sun: writing – review and editing. Yanfeng Yue: funding acquisition, project administration, supervision, conceptualization, and writing – review and editing. Stephen F. Gonski: writing – review and editing. Wei-Jun Cai: conceptualization, writing – review and editing.

Conflicts of interest

There are no conflicts of interest to declare.

Acknowledgements

This publication was made possible by the National Science Foundation EPSCoR Grant No. 1757353 and the State of Delaware.

References

1 C. L. Sabine, R. A. Feely, N. Gruber, R. M. Key, K. Lee, J. L. Bullister, R. Wanninkhof, C. S. Wong, D. W. R. Wallace, B. Tilbrook, F. J. Millero, T.-H. Peng, A. Kozyr, T. Ono and A. F. Rios, *Science*, 2004, **305**, 367–371.

2 P. Friedlingstein, M. W. Jones, M. O'Sullivan, R. M. Andrew, D. C. E. Bakker, J. Hauck, C. Le Quéré, G. P. Peters, W. Peters, J. Pongratz, S. Sitch, J. G. Canadell, P. Ciais, R. B. Jackson, S. R. Alin, P. Anthoni, N. R. Bates, M. Becker, N. Bellouin, L. Bopp, T. T. T. Chau, F. Chevallier, L. P. Chini, M. Cronin, K. I. Currie, B. Decharme, L. M. Djeutchouang, X. Dou, W. Evans, R. A. Feely, L. Feng, T. Gasser, D. Gilfillan, T. Gkritzalis, G. Grassi, L. Gregor, N. Gruber, Ö. Gürses, I. Harris, R. A. Houghton, G. C. Hurtt, Y. Lida, T. Ilyina, I. T. Luijkx, A. Jain, S. D. Jones, E. Kato, D. Kennedy, K. K. Goldewijk, J. Knauer, J. I. Korsbakken, A. Körtzinger, P. Landschützer, S. K. Lauvset, N. Lefèvre, S. Lienert, J. Liu, G. Marland, P. C. McGuire, J. R. Melton, D. R. Munro, J. E. M. S. Nabel, S.-I. Nakaoka, Y. Niwa, T. Ono, D. Pierrot, B. Poulter, G. Rehder, L. Resplandy, E. Robertson, C. Rödenbeck, T. M. Rosan, J. Schwinger, C. Schwingshackl, R. Séférian, A. J. Sutton, C. Sweeney, T. Tanhua, P. P. Tans, H. Tian, B. Tilbrook, F. Tubiello, G. R. van der Werf, N. Vuichard, C. Wada, R. Wanninkhof, A. J. Watson, D. Willis, A. J. Wiltshire, W. Yuan, C. Yue, X. Yue, S. Zaehle and J. Zeng, *Earth Syst. Sci. Data*, 2022, **14**, 1917–2005.

3 J. Blunden and D. S. Arndt, *Bull. Am. Meteorol. Soc.*, 2020, **101**, Si-S429.

4 X. Lan, P. Tans and K. W. Toning, **https://gml.noaa.gov/ccgg/trends/global.html**, (accessed 1 March 2023).

5 F. Joos and R. Spahni, *Proc. Natl. Acad. Sci. U. S. A.*, 2008, **105**, 1425–1430.

6 C. Le Quéré, R. M. Andrew, P. Friedlingstein, S. Sitch, J. Hauck, J. Pongratz, P. A. Pickers, J. I. Korsbakken, G. P. Peters, J. G. Canadell, A. Arneth, V. K. Arora, L. Barbaro, A. Nastos, L. Bopp, F. Chevallier, L. P. Chini, P. Cias, S. C. Doney, T. Gkritzalis, D. S. Goll, I. Harris, V. Haverd, F. M. Hoffman, M. Hoppema, R. A. Houghton, G. Hurtt, T. Ilyina, A. K. Jain, T. Johannessen, C. D. Jones, E. Kato, R. F. Keeling, K. K. Goldewijk, P. Landschützer, N. Lefèvre, S. Lienert, Z. Liu, D. Lombardozzi, N. Metzl, D. R. Munro, J. E. M. S. Nabel, S. Nakaoka, C. Neill, A. Olsen, T. Ono, P. Patra, A. Peregon, W. Peters, P. Peylin, B. Pfeil, D. Pierrot, B. Poulter, G. Rehder, L. Resplandy, E. Robertson, M. Rocher, C. Rödenbeck, U. Schuster, J. Schwinger, R. Séférian, I. Skjelvan, T. Steinhoff, A. Sutton, P. P. Tans, H. Tian, B. Tilbrook, F. N. Tubiello, I. T. van der Laan-Luijkx, G. R. van der Werf, N. Viovy, A. P. Walker, A. J. Wiltshire, R. Wright, S. Zaehle and B. Zheng, *Earth Syst. Sci. Data*, 2018, **10**, 2141–2194.

7 A. J. Watson, U. Schuster, J. D. Shutler, T. Holding, I. G. C. Ashton, P. Landschützer, D. K. Woolf and L. Goddijn-Murphy, *Nat. Commun.*, 2020, **11**, 4422.

8 Intergovernmental Panel on Climate Change, *Climate Change 2021: The Physical Science Basis. Contribution of Working Group I to the Sixth Assessment Report of the Intergovernmental Panel on Climate Change*, Cambridge University Press, United Kingdom and New York, NY, USA, 2021.

9 S. Barker and A. Ridgewell, *Nature Education Knowledge*, 2012, **3**, 21.

10 W.-J. Cai, Y.-Y. Xu, R. A. Feely, R. Wanninkhof, B. Jönsson, S. R. Alin, L. Barbero, J. N. Cross, K. Azetsu-Scott, A. J. Fassbender, B. R. Carter, L.-Q. Jiang, P. Pepin, B. Chen, N. Hussain, J. J. Reimer, L. Xue, J. E. Salisbury, J. M. Hernández-Ayón, C. Langdon, Q. Li, A. J. Sutton, C.-T. A. Chen and D. K. Gledhill, *Nat. Commun.*, 2020, **11**, 2691.

11 W.-J. Cai, R. A. Feely, J. M. Testa, M. Li, W. Evans, S. R. Alin, Y.-Y. Xu, G. Pelletier, A. Ahmed, D. J. Greeley, J. A. Newton and N. Bednaršek, *Annu. Rev. Mar. Sci.*, 2021, **13**, 23–55.

12 R. Zeebe, *Annu. Rev. Earth Planet. Sci.*, 2012, **40**, 141–165.

13 A. G. González, N. Pérez-Almeida, J. M. Sanatana-Casiano, F. J. Millero and M. González-Dávila, *Mar. Chem.*, 2016, **179**, 12–22.

14 R. H. Byrne, *Geochem. Trans.*, 2002, **3**, 11–16.

15 F. J. Millero, R. Woosley, B. DiTrolio and J. Water, *Oceanography*, 2009, **22**, 72–85.

16 F. M. M. Morel, A. J. Milligan and M. A. Saito, *Treatise Geochem.*, 2003, **6**, 113–143.

17 E. Brietbarth, R. J. Bellerby, C. C. Neill, M. V. Ardelan, M. Meyerhöfer, E. Zöllner, P. L. Croot and U. Riebesell, *Biogeosciences*, 2010, **7**, 1065–1073.

18 R. A. Feely, C. L. Sabine, K. Lee, W. Berelson, J. Kleypas, V. L. Fabry and F. J. Millero, *Science*, 2004, **305**, 362–366.

19 L. Cao, K. Caldeira and A. K. Jain, *Geophys. Res. Lett.*, 2007, **34**, L05607.

20 U. Riebesell, I. Zondervan, B. Rost, P. D. Tortell, R. E. Zeebe and F. M. M. Morel, *Nature*, 2000, **407**, 364–367.
21 I. Zondervan, R. E. Zeebe, B. Rost and U. Riebesell, *Global Biogeochem. Cycles*, 2001, **15**, 507–516.
22 N. R. Mollica, W. Guo, A. L. Cohen and A. R. Solow, *Proc. Natl. Acad. Sci. U. S. A.*, 2018, **115**, 1754–1759.
23 M.-D. Zheng and L. Cao, *Adv. Clim. Chang. Res.*, 2014, **5**, 189–196.
24 R. Albright, Y. Takeshita, D. A. Koweek, A. Ninokawa, K. Wolfe, T. Rivlin, Y. Nebuchina, J. Young and K. Caldeira, *Nature*, 2018, **555**, 516–519.
25 S. C. Doney, V. J. Fabry, R. A. Feely and J. A. Kleypas, *Annu. Rev. Mar. Sci.*, 2009, **1**, 169–192.
26 S. M. Bushinsky, Y. Takeshita and N. L. Williams, *Curr. Clim. Change Rep.*, 2019, **5**, 207–220.
27 Z. A. Wang, H. Moustahfid, A. V. Mueller, A. P. M. Michel, M. Mowlem, B. T. Glazer, T. A. Mooney, W. Michaels, J. S. McQuillan, J. C. Robidart, J. Churchill, M. Sourisseau, A. Daniel, A. Schaap, S. Monk, K. Friedman and P. Brehmer, *Front. Mar. Sci.*, 2019, **6**, 519.
28 Q. Shangguan, A. Prody, T. S. Wirth, E. M. Briggs, T. R. Martz and M. D. DeGrandpre, *Mar. Chem.*, 2022, **240**, 104085.
29 L. Mendecki, T. Fayose, K. A. Stockmal, J. Wei, S. Granados-Focil, C. M. McGraw and A. Radu, *Anal. Chem.*, 2015, **87**, 7515–7518.
30 R. Athavale, N. Pankratova, C. Dinkel, E. Bakker, B. Wehrli and A. Brand, *Environ. Sci. Technol.*, 2018, **52**, 11259–11266.
31 M. Cuartero, N. Pankratova, T. Cherubini, G. A. Crespo, F. Massa, F. Confalonieri and E. Bakker, *Environ. Sci. Technol. Lett.*, 2017, **4**, 410–415.
32 G. Mills and G. Fones, *Sens. Rev.*, 2012, **32**, 17–28.
33 National Academies of Sciences, *Engineering, and Medicine, A Research Strategy for Ocean-based Carbon Dioxide Removal and Sequestration*, The National Academies Press, Washington, DC, 2022.
34 D. Pines, J. Ditkovich, T. Mukra, Y. Miller, P. M. Kiefer, S. Daschakraborty, J. T. Hynes and E. Pines, *J. Phys. Chem. B*, 2016, **120**, 2440–2451.
35 W. Stumm and J. J. Morgan, in *Aquatic Chemistry: Chemical Equilibria and Rates in Natural Waters*, Wiley, 1995, pp. 157–163.
36 R. E. Zeebe and D. Wolf-Gladrow, in *CO_2 in Seawater: Equilibrium, Kinetics, Isotopes*, Elsevier, 2001, pp. 1–26.
37 M. M. Mugica, C. Day, B. McHale, K. L. McGuinness, G. Lee, D. Pickup and N. S. Lawrence, *Ocean Sci. Discuss.*, 2022, preprint, DOI: **10.5194/os-2021-126**.
38 T. Loerting and J. Bernard, *ChemPhysChem*, 2010, **11**, 2305–2309.
39 A. G. Dickson, in *Guide to best practics for ocean acidification research and data reporting*, ed. U. Riebesell, V. J. Fabry, L. Hansson and J.-P. Gattuso, Publications Office of the European Union, 2010, pp. 17–40.
40 L. D. Talley, R. A. Feely, B. M. Sloyan, R. Wanninkhof, M. O. Baringer, J. L. Bullister, C. A. Carlson, S. C. Doney, R. A. Fine, E. Firing, N. Gruber, D. A. Hansell, M. Ishii, G. C. Johnson, K. Katsumata, R. M. Key, M. Kramp, C. Langdon, A. M. Macdonald, J. T. Mathis, E. L. McDonagh, S. Mecking, F. J. Millero, C. W. Mordy, T. Nakano, C. L. Sabine, W. M. Smethie, J. H. Swift, T. Tanhua, A. M. Thurnherr, M. J. Warner and J.-Z. Zhang, *Annu. Rev. Mar. Sci.*, 2015, **8**, 185–215.
41 N. Gruber, D. Clement, B. R. Carter, R. A. Feely, S. Van Heuven, M. Hoppema, M. Ishii, R. M. Key, S. K. Lauvset, C. Lo Monaco, J. T. Mathis, A. Murata, A. Olsen, F. F. Perez, C. L. Sabine, T. Tanhua and R. Wanninkhof, *Science*, 2019, **363**, 1193–1199.
42 F. J. Millero, T. B. Graham, F. Hunag, H. Bustos-Serrano and D. Pierrot, *Mar. Chem.*, 2006, **100**, 80–94.
43 E. R. Lewis and D. W. R. Wallace, Program Developed for CO_2 System Calculations, **https://data.ess-dive.lbl.gov/view/doi:10.15485/1464255**, (accessed 10 January 2023).
44 F. J. Millero, *Geochim. Cosmochim. Acta*, 1995, **59**, 661–677.
45 D. E. Pierrot, E. Lewis and D. W. R. Wallace, *MS Excel Program Developed for CO_2 System Calculations*, **https://cdiac.ess-dive.lbl.gov/ftp/co2sys/CO2SYS_calc_XLS_v2.1/**, (accessed 10 January 2023).
46 F. J. Millero, *Chem. Rev.*, 2007, **107**, 308–341.
47 J. Ma, H. Shu, B. Yang, R. Byrne and D. Yuan, *Anal. Chim. Acta*, 2019, **1081**, 18–31.
48 J. C. Orr, J.-M. Epitalon, A. G. Dickson and J.-P. Gattuso, *Mar. Chem.*, 2018, **207**, 84–107.
49 W.-J. Cai, Y. Wang and R. E. Hodson, *Geochim. Cosmochim. Acta*, 1998, **62**, 473–483.
50 S. Song, Z. A. Wang, M. E. Gonneea, K. D. Kroeger, S. N. Chu, D. Li and H. Liang, *Geochim. Cosmochim. Acta*, 2020, **275**, 123–139.
51 K. Kuliński, B. Schneider, B. Szymczycha and M. Stokowski, *Earth Syst. Dyn*, 2017, **8**, 1107–1120.
52 O. Sulpis, S. K. Lauvset and M. Hagens, *Ocean Sci.*, 2020, **16**, 847–862.
53 M. Ramsey, *Accredit. Qual. Assur.*, 2021, **26**, 183–192.
54 E. Bakker, G. Crespo, E. Grygolowicz-Pawlak, G. Mistlberger, M. Pawlak and X. Xie, *Chimia*, 2011, **65**, 141–149.
55 S. F. Gonski, M. J. Horwith, S. Albertson, J. Bos, A. S. Brownlee, N. Coleman, C. F. Maloy, M. Keyzers, C. Krembs, G. Pelletier, E. Rauschl, H. R. Young and W.-J. Cai, *Coast. Manage.*, 2021, **49**, 487–509.
56 J. Buffle and G. Horvai, in *In Situ Monitoring of Aquatic Systems: Chemical Analysis and Speciation*, ed. J. Buffle and G. Horvai, Wiley, 2000, pp. 1–17.
57 X. Xie and E. Bakker, *Anal. Chem.*, 2013, **85**, 1332–1336.
58 Y. S. Choi, L. Lvova, J. H. Shin, S. H. Oh, C. S. Lee, B. H. Kim, G. S. Cha and H. Nam, *Anal. Chem.*, 2002, **74**, 2435–2440.
59 X. Xie, M. Pawlak, M.-L. Tercier-Waeber and E. Bakker, *Anal. Chem.*, 2012, **84**, 3163–3169.
60 M. Moßhammer, M. Strobl, M. Kühl, S. M. Borisov and K. Koren, *ACS Sens.*, 2016, **1**, 681–687.
61 E. Fritzsche, C. Staudinger, J. P. Fischer, R. Thar, H. W. Jannasch, J. N. Plant, M. Blum, G. Massion, H. Thomas, J.

Hoech, K. S. Johnson, S. M. Borisov and I. Klimant, *Mar. Chem.*, 2018, **207**, 63–76.
62 D. Atamanchuk, A. Tengberg, P. J. Thomas, J. Hovdenes, A. Apostolidis, C. Huber and P. O. J. Hall, *Limnol. Oceanogr.: Methods*, 2014, **12**, 63–73.
63 C. Staudinger, M. Strobl, J. P. Fischer, R. Thar, T. Mayr, D. Aigner, B. J. Müller, B. Müller, P. Lehner, G. Mistlberger, E. Fritzsche, J. Ehgartner, P. W. Zach, J. S. Clarke, F. Geißler, A. Mutzberg, J. D. Müller, E. P. Achterberg, S. M. Borisov and I. Kilmant, *Limnol. Oceanogr.: Methods*, 2018, **16**, 459–473.
64 M. Rosenberg, B. W. Laursen, C. G. Frankær and T. J. Sørensen, *Adv. Mater. Technol.*, 2018, **3**, 1800205.
65 M. Cuartero, *Sens. Actuators, B*, 2021, **334**, 129635.
66 M. L. Tercier, J. Buffle, A. Zirino and R. Rd. Vitre, *Anal. Chim. Acta*, 1990, **237**, 429–437.
67 S. Chaiyo, E. Mehmeti, K. Zagar, W. Siangproh, O. Chailapakul and K. Kalcher, *Anal. Chim. Acta*, 2016, **918**, 26–34.
68 X. Zhang, Y. Zhang, D. Ding, J. Zhao, J. Liu, W. Yang and K. Qu, *Microchem. J.*, 2016, **126**, 280–286.
69 S. Ma, H. Wei, D. W. Pan, F. Pan, C. C. Wang and Q. Kang, *J. Electrochem. Soc.*, 2020, **167**, 046519.
70 C. B. Jiang, Y. H. He and Y. Liu, *Analyst*, 2020, **145**, 5400–5413.
71 Y. Zhang, J. T. Nie, H. Y. Wei, H. T. Xu, Q. Wang, Y. Q. Cong, J. Q. Tao, Y. Zhang, L. L. Chu, Y. Zhou and X. Y. Wu, *Sens. Actuators, B*, 2018, **258**, 1107–1116.
72 S. Sateanchok, N. Pankratova, M. Cuartero, T. Cherubini, K. Grudpan and E. Bakker, *ACS Sens.*, 2018, **3**, 2455–2462.
73 A. V. Kolliopoulos, D. K. Kampouris and C. E. Banks, *Anal. Chem.*, 2015, **87**, 4269–4274.
74 D. Talarico, F. Arduini, A. Amine, D. Moscone and G. Palleschi, *Talanta*, 2015, **141**, 267–272.
75 S. Cinti, D. Talarico, G. Palleschi, D. Moscone and F. Arduini, *Anal. Chim. Acta*, 2016, **919**, 78–84.
76 M. M. Grand, G. S. Clinton-Bailey, A. D. Beaton, A. M. Schaap, T. H. Johengen, M. N. Tamburri, D. P. Connelly, M. C. Mowlem and E. P. Achterberg, *Front. Mar. Sci.*, 2017, **4**, 255.
77 L. Li, J. Tang, H. Liu, P. Du, Y. Zhang and Y. Qian, *SSRN*, 2022, 1–19.
78 European Marine Board, Sustaining in situ Ocean Observations in the Age of the Digital Ocean, *Zenodo*, 2021.
79 A. R. Sastri, J. R. Christian, E. P. Achterberg, D. Atamanchuk, J. J. H. Buck, P. Bresnahan, P. J. Duke, W. Evans, S. F. Gonski, B. Johnson, S. K. Juniper, S. Mihaly, L. A. Miller, M. Morley, D. Murphy, S.-i. Nakaoka, T. Ono, G. Parker, K. Simpson and T. Tsunoda, *Front. Mar. Sci.*, 2019, **6**, 653.
80 T. R. Martz, K. L. Daly, R. H. Byrne, J. H. Stillman and D. Turk, *Oceanography*, 2015, **28**, 40–47.
81 J. Buffle, K. J. Wilkinson, M.-L. Tercier and N. Parthasarathy, *Ann. Chim.*, 1997, **87**, 67–83.
82 N. P. Shetti, D. S. Nayak, K. R. Reddy and T. M. Aminabhvi, in *Micro and Nano Technologies: Graphene-Clay-Based Hybrid Nanostructures for Electrochemical Sensors and Biosensors*, ed. A. Pandikumar and P. Rameshkumar, Elsevier, 2019, pp. 235–274.
83 A. Hulanicki, S. Glab and F. Ingman, *Pure Appl. Chem.*, 1991, **63**, 1247–1250.
84 P. K. Sekhar, E. L. Brosha, R. Mukundan and F. Garzon, *Electrochem. Soc. Interface*, 2010, **19**, 35–40.
85 F. Rouessac and A. Rouessac, *Chemical Analysis: Modern Instrumentation Methods and Techniques*, John Wiley & Sons, Chichester, 2007, pp. 453–463.
86 J. Bobacka, A. Ivaska and A. Lewenstam, *Chem. Rev.*, 2008, **108**, 329–351.
87 J. Koryta, in *Ion-Selective Microelectrodes and Their Use in Excitable Tissues*, ed. E. Syková, P. Hník and L. Vyklický, Springer, Boston, MA, 1981, pp. 3–11.
88 J. J. Pedrotti, L. Angnes and I. G. R. Gutz, *Electroanalysis*, 1996, **8**, 673–675.
89 A. Yamada and M. Suzuki, *2017 International Symposium on Micro-NanoMechatronics and Human Science (MHS)*, Nagoya, Japan, 2017, pp. 1–3.
90 M. P. S. Mousavi and P. Bühlmann, *Anal. Chem.*, 2013, **85**, 8895–8901.
91 J. A. Caram, *J. Appl. Electrochem.*, 2005, **35**, 1039–1039.
92 D. C. Harris, *Quantitative Chemical Analysis*, W. H. Freeman and Company, New York, 2007, pp. 270–288.
93 D. A. Skoog, D. M. West, F. J. Holler and S. R. Crouch, in *Fundamentals of Analytical Chemistry*, Cengage, Boston, 2022, pp. 505–534.
94 P. Bühlmann and L. D. Chen, in *Supramolecular Chemistry: From Molecules to Nanomaterials*, ed. P. A. Gale and J. W. Steed, John Wiley & Sons, 2012, pp. 1–41.
95 J. R. Black, in *Encyclopedia of Geochemistry*, ed. W. White, Cham Springer, 2016, pp. 1–3.
96 Y. Soda and E. Bakker, *Sens. Actuators, B*, 2021, **346**, 130527.
97 B. N. Ciribelli, F. Colmati and E. C. de Souza, *Int. J. Innov. Educ. Res.*, 2020, **8**, 670–683.
98 C. Zhang, Y. He, J. Wu, M. Ai, W. Cai, Y. Ye, C. Tao, P. Zhang and Q. Jin, *Chemosensors*, 2021, **9**, 236.
99 E. Zdrachek and E. Bakker, *Anal. Chem.*, 2020, **92**, 2926–2930.
100 W. Gao, X. Xie and E. Bakker, *ACS Sens.*, 2020, **5**, 313–318.
101 W. Qin, T. Zwickl and E. Pretsch, *Anal. Chem.*, 2000, **72**, 3236–3240.
102 N. M. Ivanova, M. B. Levin and K. N. Mikhelson, *Russ. Chem. Bull.*, 2012, **61**, 926–936.
103 E. Bakker and E. Pretsch, *Anal. Chem.*, 2002, **74**, 420A–426A.
104 M. Püntener, T. Vigassy, E. Baier, A. Ceresa and E. Pretsch, *Anal. Chim. Acta*, 2004, **503**, 187–194.
105 A. Ceresa, T. Sokalski and E. Pretsch, *J. Electroanal. Chem.*, 2001, **501**, 70–76.
106 Q. Ye and M. E. Meyerhoff, *Anal. Chem.*, 2001, **73**, 332–336.
107 A. Zirino, R. De Marco, I. Rivera and B. Pejcic, *Electroanalysis*, 2002, **14**, 493–498.
108 T. Vigassy, R. E. Gyurcsányi and E. Pretsch, *Electroanalysis*, 2003, **15**, 1270–1275.
109 M. Cuartero and G. A. Crespo, *Curr. Opin. Electrochem.*, 2018, **10**, 98–106.

110 J. Bobacka, M. Maj-Zurawska and A. Lewenstam, *Biosens. Bioelectron.*, 2003, **18**, 245–253.
111 W. J. Scott, E. Chapoteau and A. Kumar, *Clin. Chem.*, 1986, **32**, 137–141.
112 M. Pleniceany, M. Isvoranu and C. Spinu, *J. Serb. Chem. Soc.*, 2005, **70**, 269–276.
113 D. Vlascici, S. Pruneanu, L. Olenic, F. Pogacean, V. Ostafe, V. Chiriac, E. M. Pica, L. C. Bolundut, L. Nica and E. Fagadar-Cosma, *Sensors*, 2010, **10**, 8850–8864.
114 A. W. Weber, G. D. O'Neil and S. P. Kounaves, *Anal. Chem.*, 2017, **89**, 4803–4807.
115 U.S. Integrated Ocean Observing System, *Manual for Real-Time Quality Control of pH Data Observations Version 1.0: A Guide to Quality Control and Quality of pH Data Observations*, 2019.
116 U.S. Integrated Ocean Observing System, *Manual for Real-Time Quality Control of In-situ Temperature and Salinity Data Version 2.1: A Guide to Quality Control and Quality Assurance of In-situ Temperature and Salinity Observations*, 2020.
117 L. Coppola, M. Ntoumas, R. Bozzano, M. Bensi, S. E. Hartman, M. Charcos Llorens, J. Craig, J.-F. Rolin, G. Giovanetti, D. Cano, J. Karstensen, A. Cianca, D. Toma, C. Stasch, S. Pensieri, V. Cardin, A. Tengberg, G. Petihakis and L. Cristini, *Handbook of best practices for open ocean fixed observatories*, European Commission, 2016.
118 S. Lauvset, K. Currie, N. Metzl, S.-i. Nakaoka, D. Bakker, K. Sullivan, A. Sutton, K. O'Brien and A. Olsen, SOCAT Quality Control Cookbook for SOCAT version 7, **https://repository.oceanbestpractices.org/bitstream/handle/11329/1755/2018_SOCAT_QC_Cookbook_final_with-v2021-contact-details.pdf?sequence=1&isAllowed=y**, (accessed 13 January 2023).
119 C. Han, W.-J. Cai, Y. Wang and Y. Ye, *J. Oceanogr.*, 2014, **70**, 425–433.
120 W. M. Wise, *U.S. Pat.*, 3723281, 1973.
121 H. B. Herman and G. A. Rechnitz, *Anal. Chim. Acta*, 1975, **76**, 155–164.
122 W. Simon, E. Pretsch, W. E. Morf, D. Ammann, U. Oesch and O. Dinten, *Analyst*, 1984, **109**, 207–209.
123 J. J. Jasielec, T. Sokalski, R. Filipek and A. Lewenstam, *Anal. Chem.*, 2015, **87**, 8665–8672.
124 S. Makarychev-Mikhailov, A. Legin, J. Mortensen, S. Levitchev and Y. Vlasov, *Analyst*, 2004, **129**, 213–218.
125 E. A. Materova, T. Y. Bart, E. V. Soboleva, V. S. Karavan and L. O. Ishutkina, *Electrokhimiya*, 1981, **17**, 499.
126 T. Katsu and N. Hanada, *Anal. Chim. Acta*, 1996, **321**, 21–25.
127 T. Katsu and Y. Mori, *Talanta*, 1996, **43**, 755–759.
128 K. Watanabe, O. Noguchi, K. Okada and T. Katsu, *Anal. Sci.*, 1997, **13**, 209–212.
129 S. Sasaki, A. Hashizume, D. Citterio, E. Fujii and K. Suzuki, *Angew. Chem., Int. Ed.*, 2002, **41**, 3005–3007.
130 A. L. Smirnova, V. N. Tarasevitch and E. M. Rakhman'ko, *Sens. Actuators, B*, 1994, **19**, 392–395.
131 V. L. Khitrova, N. B. Ivanenko, V. S. Karavan, E. M. Rakhman'ko and A. L. Smirnova, *Russ. J. Appl. Chem.*, 1997, **70**, 962.
132 K. N. Mikhelson, A. L. Smirnova and N. A. Malysh, *Electrokhimiya*, 1994, **30**, 1109.
133 W. J. Scott, E. Chapoteau and A. Kumar, *Clin. Chem.*, 1986, **32**, 137–141.
134 E. M. Rakhman'ko, A. L. Gulevich, A. P. Podterob and P. V. Senin, *Zh. Anal. Khim.*, 1998, **53**, 1–4.
135 M. E. Meyerhoff, E. Pretsch, D. H. Welti and W. Simon, *Anal. Chem.*, 1987, **59**, 144–150.
136 S. Makarychev-Mikhailov, O. Goryacheva, J. Mortensen, A. Legin, S. Levitchev and Y. Vlasov, *Electroanalysis*, 2003, **15**, 1291–1296.
137 C. Behringer, B. Lehmann, J.-P. Haug, K. Seiler, W. E. Morf, K. Hartman and W. Simon, *Anal. Chim. Acta*, 1990, **233**, 41–47.
138 T. Sokalski, D. Paradowski, J. Ostaszewska, M. Maj-Zurawska, J. Mieczkowski, A. Lewenstam and A. Hulanicki, *Analyst*, 1996, **121**, 133–138.
139 M. Maj-Zurawska, T. Sokalski, J. Ostaszewska, D. Paradowski, J. Mieczkowski, Z. Charnocki, A. Lewenstam and A. Hulanicki, *Talanta*, 1997, **44**, 1641–1647.
140 A. K. Jain, V. K. Gupta and J. R. Raisoni, *Electrochim. Acta*, 2006, **52**, 951–957.
141 V. Thimaradka, S. Pangannaya, M. Mohan and D. R. Trivedi, *Spectrochim. Acta A Mol. Biomol. Spectrosc.*, 2017, **193**, 330–337.
142 A. Singh, M. Mohan and D. R. Trivedi, *ChemistrySelect*, 2019, **4**, 14120–14131.
143 H. J. Pyun, J. Chu, Y. M. Jun and D. J. Kim, *Bull. Korean Chem. Soc.*, 1999, **20**, 112–116.
144 H. J. Pyun, J. Chu, W. J. Yoon, Y. M. Jun and D. J. Kim, *Bull. Korean Chem. Soc.*, 1999, **20**, 179–186.
145 H. J. Lee, I. J. Yoon, C. L. Yoo, H. J. Pyun, G. S. Cha and H. Nam, *Anal. Chem.*, 2000, **72**, 4694–4699.
146 J. H. Shim, I. S. Jeong, M. H. Lee, H. P. Hong, J. H. On, K. S. Kim, H. S. Kim, B. H. Kim, G. S. Cha and H. Nam, *Talanta*, 2004, **63**, 61–71.
147 F. Song, J. Ha, B. Park, T. H. Kwak, I. T. Kim, H. Nam and G. S. Cha, *Talanta*, 2002, **57**, 263–270.
148 D. de Beer, A. Bissett, R. de Wit, H. Jonkers, S. Köhler-Rink, H. Nam, B. H. Kim, G. Eickert and M. Grinstain, *Limnol. Oceanogr.: Methods*, 2008, **6**, 532–541.
149 W. J. Cai, Y. Ma, B. M. Hopkinson, A. G. Grottoli, M. E. Warner, Q. Ding, X. Hu, X. Yuan, V. Schoepf, H. Xu, C. Han, T. F. Melman, K. D. Hoadley, D. T. Pettay, Y. Matsui, J. H. Baumann, S. Levas, Y. Ying and Y. Wang, *Nat. Commun.*, 2016, **7**, 11144.
150 Z. Jarolímová, J. Bosson, G. M. Labrador, J. Lacour and E. Bakker, *Electroanalysis*, 2018, **30**, 1378–1385.
151 L. D. Chen, D. Mandal, G. Pozzi, J. A. Gladysz and P. Bühlmann, *J. Am. Chem. Soc.*, 2011, **133**, 20869–20877.
152 K. N. Mikhelson and M. A. Peshkova, *Russ. Chem. Rev.*, 2015, **84**, 555–578.
153 R. A. Durst, in *Ion-Selective Electrodes in Analytical Chemistry*, ed. H. Freiser, Springer New York, NY, 1978, pp. 311–338.
154 B. P. Nikol'skii and E. A. Materova, *Ionoselektivnye Elektrody*, Khimiya, Leningrad, 1980.
155 A. Kisiel, E. Woźnica, M. Wojciechowski, E. Bulska, K. Maksymiuk and A. Michalska, *Sens. Actuators, B*, 2015, **207**, 995–1003.

156 G. J. Moody, R. B. Oke and J. D. R. Thomas, *Analyst*, 1970, **95**, 910–918.
157 N. Vladimirova, V. Polukeev, J. Ashina, V. Babain, A. Legin and D. Kirsanov, *Chemosensors*, 2022, **10**, 43.
158 J. Pick, K. Tóth, M. Vasàk, E. Pungor and W. Simon, *Anal. Chim. Acta*, 1973, **64**, 477–480.
159 U. Fiedler and J. Růžička, *Anal. Chim. Acta*, 1973, **67**, 179–193.
160 F. Faridbod, M. R. Ganjali, R. Dinarvand and P. Norouzi, *Afr. J. Biotechnol.*, 2007, **6**, 2960–2987.
161 P. Zhao and W.-J. Cai, *Anal. Chim. Acta*, 1999, **395**, 285–291.
162 J. H. Shin, D. S. Sakong, H. Y. Nam and G. S. Cha, *Anal. Chem.*, 1996, **68**, 221–225.
163 S. C. Ma, N. A. Chaniotakis and M. E. Meyerhoff, *Anal. Chem.*, 1988, **60**, 2293–2299.
164 Z. Pingsan and W.-J. Cai, *Anal. Chem.*, 1997, **69**, 5052–5058.
165 Y. Qin and E. Bakker, *Anal. Chem.*, 2001, **73**, 4262–4267.
166 S. Dabrowska, J. Migdalski and A. Lewenstam, *Electroanalysis*, 2017, **29**, 140–145.
167 B. H. Kim, C. S. Lee, J. H. Shim, H. P. Hong, G. S. Cha, Y. M. Jun and H. Nam, *Talanta*, 2003, **61**, 393–401.
168 X. Dong, D. Lu, T. A. L. Harris and I. C. Escobar, *Membranes*, 2021, **11**, 309.
169 U. Oesch and W. Simon, *Anal. Chem.*, 1980, **52**, 692–700.
170 O. H. LeBlanc Jr. and W. T. Grubb, *Anal. Chem.*, 1976, **48**, 1658–1660.
171 R. Eugster, P. M. Gehrig, W. E. Morf, U. E. Spichiger and W. Simon, *Anal. Chem.*, 1991, **63**, 2285–2289.
172 E. Bakker, P. Bühlmann and E. Pretsch, *Chem. Rev.*, 1997, **97**, 3083–3132.
173 K. N. Mikhelson, *Ion-Selective Electrodes (Lecture Notes in Chemistry)*, Springer, Heidelberg, New York, Dordrecht, London, 2013.
174 U. Shaller, E. Bakker, U. E. Spichiger and E. Pretsch, *Anal. Chem.*, 1994, **66**, 391–398.
175 P. Bühlmann, S. Amemiya, S. Yajima and Y. Umezawa, *Anal. Chem.*, 1998, **70**, 4291–4303.
176 K. N. Mikhelson and A. Lewenstam, *Sens. Actuators, B*, 1998, **48**, 344–350.
177 K. N. Mikhelson and A. Lewenstam, *Anal. Chem.*, 2000, **72**, 4965–4972.
178 S. E. Didina, O. P. Chogin, K. N. Mikhelson and A. Levenstam, *Vestn. S.-Peterb. Univ.*, 1999, **4**, 39.
179 D. Ammann, *Ion-Selective Microelectrodes: Principles, Design and Application*, Springer, Berlin, Heidelberg, New York and Tokyo, 1986.
180 E. Linder and R. E. Gyurcsányi, *J. Solid State Electrochem.*, 2009, **13**, 51–68.
181 R. W. Baker, *Membrane Technology and Applications*, John Wiley & Sons, Inc., New York, 2012.
182 J. Ren and R. Wang, in *Membrane and Desalination Technologies: Handbook of Environmental Engineering*, ed. L. K. Wang, J. P. Chen, Y. T. Hung and N. K. Shammas, Humana Press, Totowa, NJ, 2011, pp. 47–100.
183 C. Das and K. A. Gebru, *Polymeric Membrane Synthesis, Modification, and Applications: Electro-Spun and Phase Inverted Membranes*, CRC Press, Boca Raton, 2018.
184 T. Sokalski, M. Maj-Zurawska and A. Hulanicki, *Microchim. Acta*, 1991, **1**, 285–291.
185 T. Sokalski, A. Ceresa, T. Zwickl and E. Pretsch, *J. Am. Chem. Soc.*, 1997, **119**, 11347–11348.
186 R. E. Gyurcsanyi, E. Pergel, R. Nagy, I. Kapui, B. T. T. Lan, K. Toth, I. Bitter and E. Lindner, *Anal. Chem.*, 2001, **73**, 2104–2111.
187 S. Amemiya, P. Bühlmann and Y. Umezawa, *Anal. Chem.*, 1998, **70**, 445–454.
188 P. Bühlmann and Y. Umezawa, *Electroanalysis*, 1999, **11**, 687–693.
189 E. Steinle, S. Amemiya, P. Bühlmann and M. Meyerhoff, *Anal. Chem.*, 2000, **72**, 5766–5773.
190 S. Amemiya, P. Bühlmann and K. Odashima, *Anal. Chem.*, 2003, **75**, 3329–3339.
191 S. S. Koseoglu, C.-Z. Lai, C. Ferguson and P. Bühlmann, *Electroanalysis*, 2008, **20**, 331–339.
192 M. Miyake, L. D. Chen, G. Pozzi and P. Bühlmann, *Anal. Chem.*, 2012, **84**, 1104–1111.
193 T. Blaz, J. Migdalski and A. Lewenstam, *Analyst*, 2005, **130**, 637–643.
194 International Organization for Standardization, *Capability of Detection*, Genève, Switzerland, 2000.
195 D. MacDougall and W. B. Crummett, *Anal. Chem.*, 1980, **52**, 2242–2249.
196 T. Sokalski, A. Ceresa, M. Fibbioli, T. Zwickl, E. Bakker and E. Pretsch, *Anal. Chem.*, 1999, **71**, 1210–1214.
197 D. Yuan, A. H. C. Anthis, M. G. Afshar, N. Pankratova, M. Cuartero, G. A. Crespo and E. Bakker, *Anal. Chem.*, 2015, **87**, 8640–8645.
198 J. Vessman, R. I. Stefan, J. F. van Staden, K. Danzer, W. Linder, D. T. Burns, A. Fajgeji and H. Müller, *Pure Appl. Chem.*, 2001, **73**, 1381–1386.
199 B. Zang, H. Tang, Z. Zhao and S. Song, *ACS Omega*, 2020, **5**, 6229–6239.
200 Y. Umezawa, P. Bühlmann, K. Umezawa, K. Tohda and S. Amemiya, *Pure Appl. Chem.*, 2000, **72**, 1851–2082.
201 R. P. Buck and E. Lindner, *Pure Appl. Chem.*, 1994, **66**, 2527–2536.
202 V. V. Egorov, E. A. Zdrachek and V. A. Nazarov, *Anal. Chem.*, 2014, **86**, 3693–3696.
203 K. Hiiro, S.-I. Wakida and M. Yamane, *Anal. Sci.*, 1988, **4**, 149–151.
204 A. Merikhi, P. Berg, V. Meyer and M. Huettel, *Limnol. Oceanogr.: Methods*, 2018, **16**, 475–483.
205 C. Macca, *Anal. Chim. Acta*, 2004, **512**, 183–190.
206 Z. Sun, Q. Ma, Y. Wang and Y. Pan, *J. Electrochem. Soc.*, 2020, **167**, 047501.
207 R. Athavale, I. Kokorite, C. Dinkel, E. Bakker, B. Wehrli, G. A. Crespo and A. Brand, *Anal. Chem.*, 2015, **87**, 11990–11997.
208 R. Athavale, C. Dinkel, B. Wehrli, E. Bakker, G. A. Crespo and A. Brand, *Environ. Sci. Technol. Lett.*, 2017, **4**, 286–291.

209 J. Su, Y. Liu, Y. Song, L. Huang, W. Guo, X. Cao, Y. Dou, L. Chang, G. Li, Q. Hu and R. Ye, *SmartMat*, 2022, **3**, 35–53.
210 Z. Sun, H. Yin, K. Liu, S. Cheng, G. K. Li, S. Kawi, H. Zhao, G. Jia and Z. Yin, *SmartMat*, 2022, **3**, 68–83.
211 Z. Gao, M. Hou, Y. Shi, L. Li, Q. Sun, S. Yang, Z. Jiang, W. Yeng, Z. Zheng and W. Hu, *Chem. Sci.*, 2023, **14**, 6860–6866.
212 M. Hou, Y. x. Shi, J. j. Li and Z. Gao, *Chem. – Asian J.*, 2022, **17**, e202200624.